

3. PARAMETRIC SYSTEMS STUDIES AND DESIGN-POINT SELECTION

Ronald L. Miller

Robert A. Krakowski

Contents

3.1.	INTRODUCTION	3-1
3.2.	MODELS	3-6
3.2.1.	Plasma Physics Model	3-6
3.2.2.	Reactor Engineering Model	3-16
3.3.	COSTING	3-23
3.4.	TITAN-I DESIGN POINT	3-32
3.4.1.	Design Point Selection	3-32
3.4.2.	Trade-off and Sensitivity Studies	3-43
3.5.	TITAN-II DESIGN POINT	3-53
3.5.1.	Design-Point Selection	3-53
3.5.2.	Trade-off and Sensitivity Studies	3-57
3.6.	SUMMARY AND CONCLUSIONS	3-57
	REFERENCES	3-64

3. PARAMETRIC SYSTEMS STUDIES AND DESIGN-POINT SELECTION

3.1. INTRODUCTION

The objective of the systems analysis activity is the systematic study and determination of plant operating parameters through economic analysis and optimization of the power station, emphasizing the performance of the fusion power core. The fusion power core (FPC) includes the plasma chamber, first wall, blanket, shield, coils, and associated structure. The reference design points are chosen to meet overall design goals of the TITAN study such as minimal cost of electricity (COE) and high mass power density (MPD). In addition to the reference design points, trade-off and sensitivity studies were performed to establish and characterize the “design window” for attractive RFP reactor operation.

A parametric systems analysis (PSA) computer code is used for this study. This code was originally developed for use in the Los Alamos compact reversed-field pinch reactor (CRFPR) studies [1 - 3], and the cost data base was updated in the course of the Los Alamos modular stellarator reactor, MSR [4] and spherical torus reactor, ATR/ST [5] studies. Further updates of the cost data base made in the course of the TITAN study are discussed in Section 3.3. Code models include steady-state surveys designed to assess sensitivities and trade-offs related to various TITAN operating configurations and assumptions. These models are benchmarked and calibrated against more detailed plasma physics and magnetics models to provide a framework for the overall design process (Figure 3.1-1).

The PSA code algorithm used in the CRFPR study (Figure 6.1 of Reference [3]) has been modified to treat the equilibrium-field (EF) and ohmic-heating (OH) coil sets separately, allowing the consideration of superconducting EF coils. As indicated on Figure 3.1-2, the PSA code identifies optimal reactor parameters for a specified net electric power, P_E , using a set of nested search loops centered on a convergence operation for the engineering Q-value, $Q_E = 1/\epsilon$, where ϵ is the recirculating power fraction. This innermost iteration procedure searches for the value of Q_E that yields the specified P_E for a given total coil thickness, δ_c , as the split between the toroidal-field (TF) coil and OH coil geometry is varied.

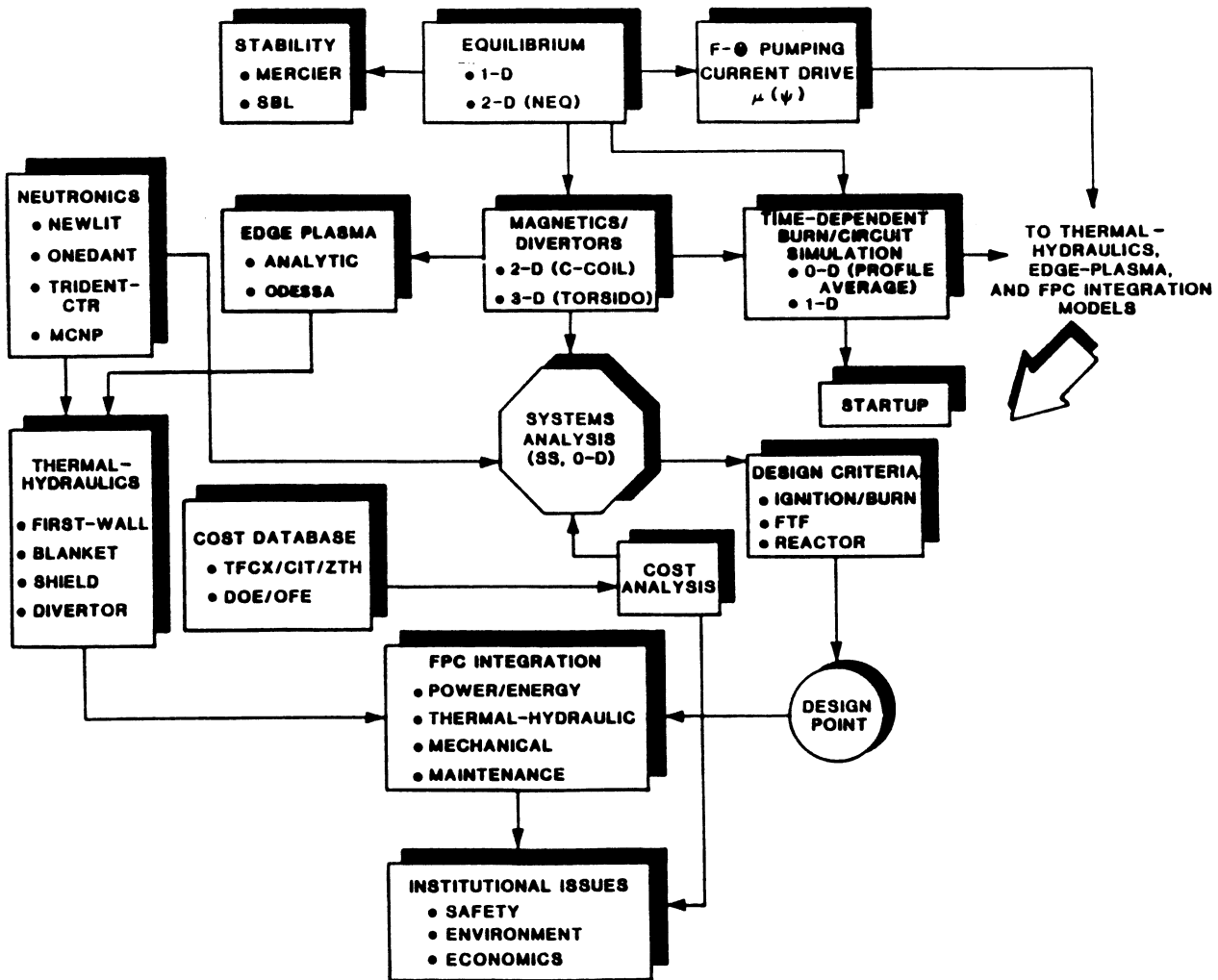


Figure 3.1-1. TITAN study approach organized by key plasma and nuclear engineering activities and interfaces. Some of the computer codes used in the TITAN study are NEQ [6,7], NEWLIT [8], ONEDANT [9], TRIDENT-CTR [10], MCNP [11], CCOIL [2], TORSIDO [4], and ODESSA [12].

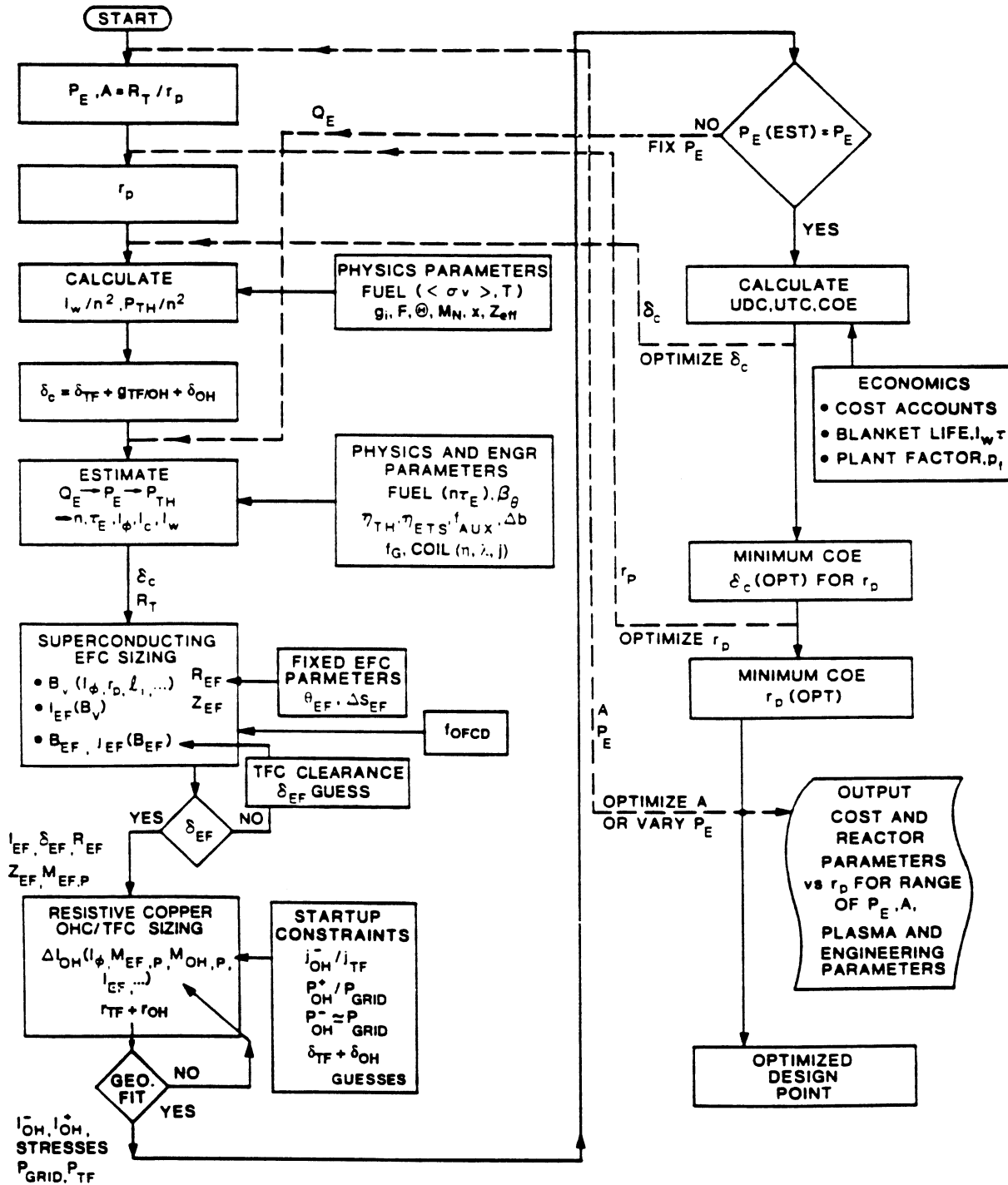


Figure 3.1-2. Parametric systems analysis (PSA) procedure used for the TITAN study, as adapted from CRFPR study methods [1-3].

First, for a fixed geometry (including plasma major and minor radii and aspect ratio), the inner loop finds the total TF coil and OH coil thickness, δ_c , which produces a minimum-COE design for the specified P_E . This procedure is repeated for different values of plasma minor radius, r_p , to determine a higher-order (lower) COE minimum. Generally, r_p is used as a display variable, with the respective minimum-COE design corresponding to a particular value of P_E and plasma aspect ratio, $A \equiv R_T/r_p$ (R_T is the plasma major radius). The outermost loop then varies A in search of an even lower minimum-COE system although, within realistic bounds, the optimum in A is found to be relatively flat for the RFP. These fully cost-optimized design points are then examined as a function of P_E and various physics, engineering, and economic parameters and options. The results of this analysis identify preliminary design points which serve as the starting points for engineering analysis. As this subsequent analysis characterizes the global performance of various subsystems, the optional parameters of the PSA code are updated to provide an evolving, self-consistent picture of the TITAN design points.

The PSA model geometry is illustrated in Figure 3.1-3. A moderate aspect-ratio plasma is surrounded by a first-wall with radius, r_w . A conventional design fits a blanket and shield annulus around the first wall followed by a resistive copper-alloy TF coil set and a dominant resistive OH-coil set. An EF-coil set could be either superconducting or normal conducting. The former option (used for TITAN) requires additional local radiation shielding. The integrated blanket coil (IBC) option [13] is used in TITAN-I (Section 3.4) which consolidates the TF-coil set with the blanket.

The PSA code initialization section, executed prior to the (A, P_E) search loops, establishes the plasma physics conditions. A plasma density-weighted, volume-averaged temperature, T ($T_e \simeq T_i$), and corresponding Lawson parameter, $n_i \tau_E$, are selected. The radial profiles of plasma temperature, density, and $\mu(r) \equiv \mu_o \mathbf{j} \cdot \mathbf{B}/B^2$ are obtained from empirical fits to the results of 1-D RFPBURN plasma simulations (Section 5.3). The ratio of electron to ion density, n_e/n_i , is calculated from an input value of Z_{eff} .

Other input values include the poloidal beta, $\beta_\theta \simeq 2\mu_o k_B (n_e + n_i) T / \bar{B}_\theta^2(r_p)$, the reversal parameter, $F = \bar{B}_\phi(r_p) / \langle B_\phi \rangle$, and a representative value of toroidal plasma current, I_ϕ . Here μ_o is the permeability of free space, $k_B = 1.602 \times 10^{-16}$ J/keV is the Boltzmann constant, $\bar{B}_\theta(r)$, $\bar{B}_\phi(r)$ denote, respectively, the flux-surface-averaged poloidal and toroidal magnetic field, and $\langle B_\phi \rangle$ is the volume-averaged toroidal field. From these input values, a self-consistent value of the pinch parameter, $\Theta = \bar{B}_\theta(r_p) / \langle B_\phi \rangle$, and the profile enhancement (of fusion power, Bremsstrahlung, and ohmic heating) factors, g_j , are computed using a numerical equilibrium solver (Section 5.2) and the assumed plasma density, temperature, and μ profiles.

The magnitude of the plasma current, I_ϕ , is adjusted within the (A, P_E) search loops, as required. For a fixed value of $n_i\tau_E$, the ion density is adjusted to yield the required fusion power, P_F , and neutron wall load, I_w . For each particular geometric configuration, the cost-optimized confinement time, $\tau_E(\text{OPT})$, is determined at the minimum-COE design point. These values of $\tau_E(\text{OPT})$ are then compared with $\tau_E(\text{PHYS}) \propto I_\phi^\nu$ (Section 3.2) to assess the accessibility of the tentative design point.

Section 3.2 summarizes the physics and engineering models used in the PSA code. Section 3.3 describes the costing algorithms. The TITAN-I and TITAN-II design points and sensitivities studies are presented in Sections 3.4 and 3.5, respectively. A summary of the results of the systems-studies activity is given in Section 3.6.

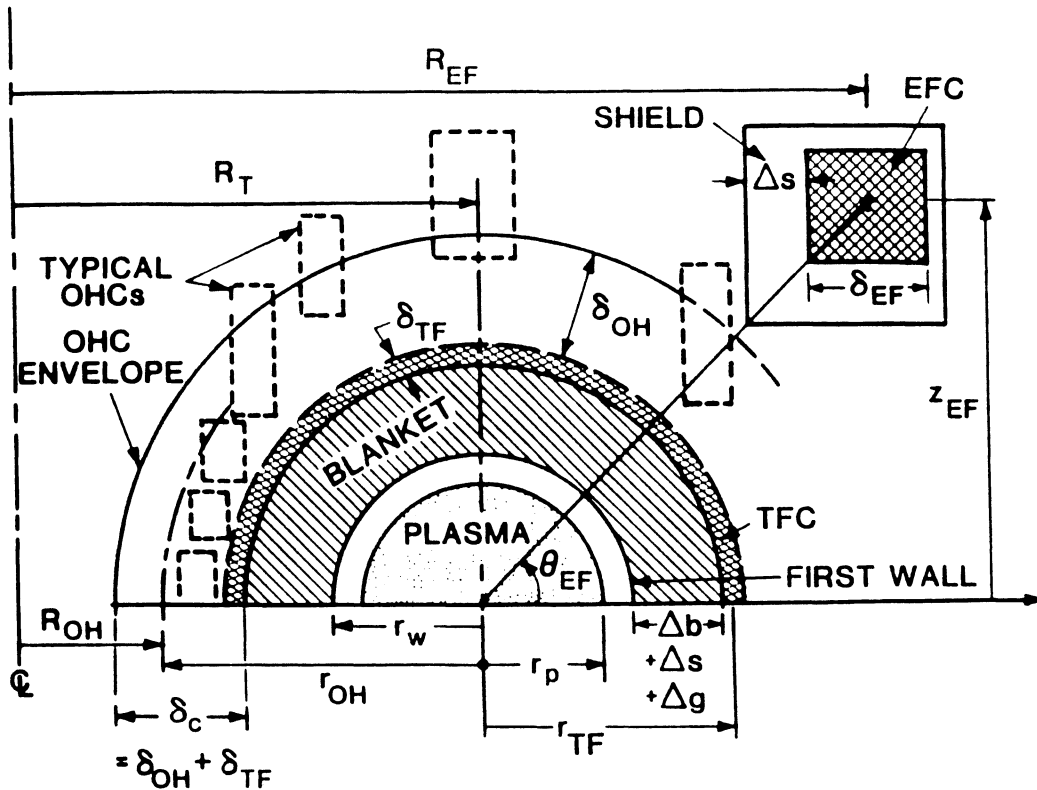


Figure 3.1-3. The FPC model used to optimize and perform sensitivity studies of TITAN reactors. The computational model loops through all FPC and plasma dimensions in search of minimum-COE designs. The IBC option [13] combines the TF-coil set with the blanket in TITAN-I.

3.2. MODELS

3.2.1. Plasma Physics Model

An RFP plasma is confined by a combination of a poloidal field, B_θ , generated by a toroidal current, I_ϕ , flowing in the plasma, and a toroidal field, B_ϕ , produced partly by currents flowing in the plasma and partly by external coils. The distinguishing features of the RFP are: (a) $B_\theta \simeq |B_\phi|$ within the plasma, and (b) the toroidal field is reversed and much smaller in magnitude in the outer region with respect to the value on the axis. A fundamental property of the RFP is that the field configuration and the generation of the reversed toroidal field is a natural consequence of the relaxation of the plasma to a near-minimum-energy state. This relaxation process results in a close coupling of poloidal and toroidal circuits through the plasma and allows the use of oscillating-field current drive (OFCD) for steady-state sustainment. The RFP edge safety factor, $q = r_p B_\phi / R_T B_\theta$, is less than unity, creating the possibility of large plasma current density, strong ohmic heating, and low magnetic fields at coils. Typical values of poloidal beta, β_θ , equal or exceed 0.20, allowing high plasma DT-fusion power densities ($> 70 \text{ MW/m}^3$). Energy confinement is assumed to scale as $\tau_E \propto I_\phi^\nu r_p^2$, where $\nu \simeq 1.0$. These inherent characteristics of the RFP confinement concept lead to a high-power-density, steady-state plasma configuration with a relatively weak external toroidal field and promise an improved commercial reactor.

The TITAN systems model begins with a steady-state, point-plasma model, corrected for profile effects. It is convenient to define a plasma-filling fraction, $x \equiv r_p / r_w$, for the circularized plasma in a toroidal chamber, where r_w is the minor radius of the first wall and r_p is the plasma-core radius (*i.e.*, to the separatrix). The parameter x is chosen to anticipate the first-wall geometry and scrape-off layer thickness ($r_w - r_p$) in relating the volumetric fusion power to the average 14.1-MeV neutron first-wall load.

The average plasma DT-fusion (17.58 MeV/fusion) power density, P_F/V_p , is given by

$$P_F/V_p \text{ (W/m}^3\text{)} = 2.186 \times 10^{-12} g_{DT} n_D n_T \langle \sigma v \rangle_{DT}, \quad (3.2-1)$$

where $n_{D,T}$ is the average DT fuel-ion density ($n_{D,T} = f_{D,T} n_i$), n_i is the total ion density, and g_{DT} is the fusion-power profile correction factor. The values for the DT fusion reactivity, $\langle \sigma v \rangle_{DT}$, are based on the recent Los Alamos experimental measurements and temperature-dependent fitting function [14] in the range $0 < T < 20 \text{ keV}$, with typical results summarized in Table 3.2-I.

Table 3.2-I.
MAXWELLIAN-AVERAGED DT FUSION REACTIVITIES [14]

Temperature, T (keV)	Reactivity, $\langle\sigma v\rangle$ (m ³ /s)	$\langle\sigma v\rangle/T^2$ (m ³ /s-keV ²)
0.5	5.58×10^{-29}	2.23×10^{-28}
1.0	6.71×10^{-27}	6.71×10^{-27}
5.0	1.33×10^{-23}	5.30×10^{-25}
10.0	1.12×10^{-22}	1.12×10^{-24}
13.5	2.21×10^{-22}	1.215×10^{-24} ^(a)
15.0	2.71×10^{-22}	1.20×10^{-24}
20.0	4.29×10^{-22}	1.07×10^{-24}
25.0 ^(b)	5.95×10^{-22}	9.52×10^{-25}

(a) Maximum value.

(b) Out of the nominal range of the fitting function used.

Differences in physics assumptions between the TITAN study and earlier CRFPR studies [2,3] are summarized in Table 3.2-II. For purposes of the TITAN study, a lower value of poloidal beta, β_θ , and flatter radial profiles of plasma temperature and density have been assumed (the flatter profiles are a result of 1-D RFPBURN-code plasma simulations, described in Section 5.3). These profiles are displayed in Figure 3.2-1. The g values reported in Table 3.2-II measure the peaked profile enhancement of fusion power (g_{DT}), ohmic heating (g_{OHM}), and Bremsstrahlung (g_{BR}) relative to the values obtained from flat profiles.

Generally, the volume-averaged power densities are given by

$$P_j \equiv \langle P_j(r) \rangle = \langle f_j[B(r), j(r), n(r), T(r)] \rangle, \quad (3.2-2)$$

where the subscript j denotes fusion, radiation, or ohmic-heating power density. The systems model calculates volume-average power densities, P_j , using average parameters;

Table 3.2-II.
COMPARISON OF PHYSICS PARAMETERS
OF RFP REACTOR STUDIES

Parameter	CRFPR [2,3]	TITAN
$\mu(r)/\mu(0)$	$\begin{cases} 1 & (r < r^*) \\ \frac{r_p - r}{r_p - r^*} & (r^* < r < r_p) \end{cases}$	(Section 5.3) ^(a)
$T(r)/T(0)$	$J_0(\mu r)$	(Section 5.3) ^(a)
$n(r)/n(0)$	$J_0(\mu r)$	(Section 5.3) ^(a)
Ion temperature, T_i (keV)	10.	10.
Electron temperature, T_e (keV)	10.	9.5
Poloidal beta, β_θ	0.20	0.20 (0.22) ^(b)
Pinch parameter, Θ	1.55	1.556
Reversal parameter, F	-0.12	-0.10
Fusion reactivity enhancement, g_{DT}	2.23	1.403
Ohmic-heating enhancement, g_{OHM}	5.08	2.924
Bremsstrahlung enhancement, g_{BR}	1.52	1.172
Lawson parameter, $n\tau_E$, (s/m ³) ^(c)	1.60×10^{20}	1.92×10^{20}
Effective plasma charge, Z_{eff} ^(d)	~ 1.0	1.69 ^(d)

(a) Profiles of plasma parameters from 1-D simulations of Section 5.3.

(b) Includes contribution of fusion-product alpha particles ($E_\alpha \simeq 60$ keV) and impurities ($T_{Xe} = T_i = 10$ keV).

(c) At $T \simeq 10$ keV.

(d) $Z_{eff} \equiv \sum n_j Z_j^2 / \sum n_j Z_j$, where j denotes the ion species.

Defining $f_j = n_j/n_i$, typically $f_{D,T} = f_T = f_D = 0.48484$, $f_\alpha = 0.0030$, and $f_{Xe} = 0.00033$ with $Z_{Xe} = 45$ for the partially stripped Xe impurity ions.

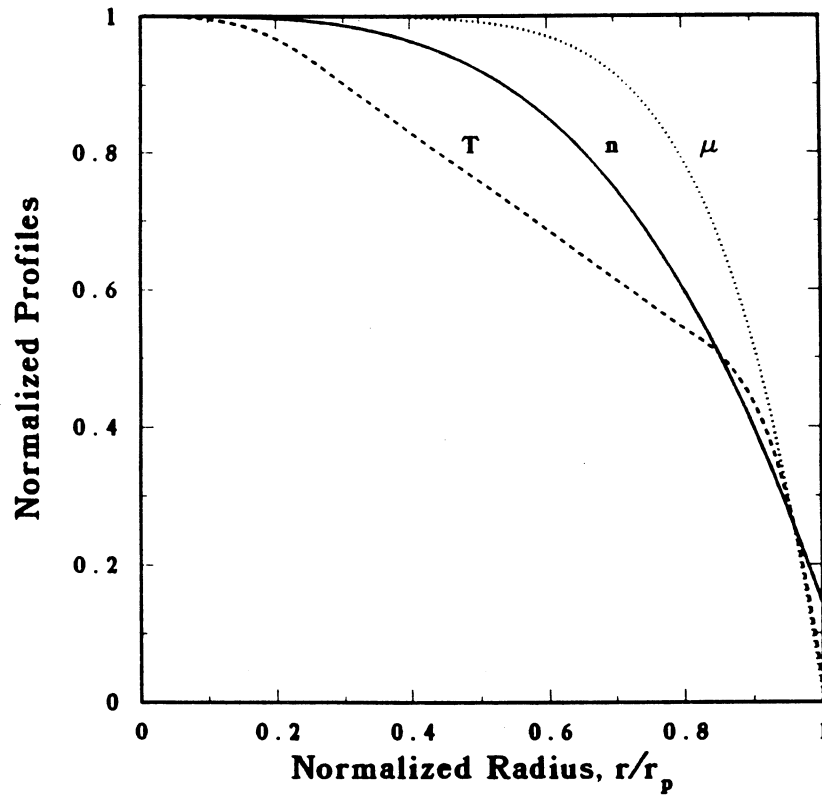


Figure 3.2-1. Profiles of core-plasma normalized density, n , temperature, T , and $\mu = \mu_o \mathbf{j} \cdot \mathbf{B}/B^2$ as obtained from 1-D simulations (Section 5.3).

all profile information is contained in the profile-enhancement factors g_j , where

$$P_j = g_j f_j(\langle B \rangle, \langle j \rangle, \langle n \rangle, \langle T \rangle). \quad (3.2-3)$$

Henceforth, these quantities are volume-averaged and $\langle \rangle$ is dropped except otherwise specified so that the notation can be simplified.

The average current density, plasma density, and temperature used in Equation 3.2-1 are defined as follows:

$$j_\phi \equiv \frac{I_\phi}{A_p}, \quad (3.2-4)$$

$$n \equiv \frac{2\pi}{A_p} \int_0^{r_p} n(r) r dr, \quad (3.2-5)$$

$$T \equiv \frac{2\pi}{n A_p} \int_0^{r_p} T(r) n(r) r dr, \quad (3.2-6)$$

where I_ϕ is the toroidal plasma current and $A_p = \pi r_p^2$ is the plasma minor cross-sectional area. The profile factors are then defined as

$$g_j \equiv \frac{2\pi}{P_j A_p} \int_0^{r_p} P_j(r) r dr . \quad (3.2-7)$$

The ohmic-heating profile correction factor, for example, becomes

$$g_{OHM} = \frac{2\pi}{\eta_{||}(n, T) I_\phi^2 A_p} \int_0^{r_p} \eta_{||} [n(r), T(r)] [j_\phi^2(r) + j_\theta^2(r)] r dr , \quad (3.2-8)$$

where $\eta_{||}$ is the classical Spitzer resistivity ($\propto Z_{eff} T_e^{-3/2}$).

The profiles of fields and current densities in the plasma are found using the ideal MHD equations,

$$\nabla \times \mathbf{B} = \mu_o \mathbf{j} = \mu_o (\mathbf{j}_{||} + \mathbf{j}_\perp) , \quad (3.2-9)$$

$$\mathbf{j} \times \mathbf{B} = \nabla p , \quad (3.2-10)$$

where $\mathbf{j}_{||}$ and \mathbf{j}_\perp are, respectively, the components of the current density parallel and perpendicular to the magnetic field. It is the natural tendency for the RFP configuration to relax to a force-free Woltjer-Taylor minimum-energy state [15,16]. These relaxed states are characterized by the reversal parameter, F , the pinch parameter, Θ , and the parameter $\mu(r)$, where

$$F \equiv \frac{\bar{B}_\phi(r_p)}{\langle B_\phi \rangle} , \quad (3.2-11)$$

$$\Theta \equiv \frac{\bar{B}_\theta(r_p)}{\langle B_\phi \rangle} , \quad (3.2-12)$$

$$\mu(r) \equiv \frac{\mu_o \mathbf{j}(r) \cdot \mathbf{B}(r)}{B^2} , \quad (3.2-13)$$

with \bar{B}_ϕ and \bar{B}_θ being flux-surface-averaged quantities. Typically, $\mu(r)$ is constant within the central plasma and decreases to zero across the cold plasma edge, where the highly resistive edge plasma cannot support large current densities.

The parallel and perpendicular component of the current density can be found, respectively, from the definition of $\mu(r)$ (Equation 3.2-13) and the ideal MHD pressure-balance Equation 3.2-10 to be

$$\mathbf{j}_{||} = \frac{(\mathbf{j} \cdot \mathbf{B}) \mathbf{B}}{B^2} = \mu(r) \mathbf{B} , \quad (3.2-14)$$

$$\mathbf{j}_\perp = \frac{\nabla p \times \mathbf{B}}{B^2} . \quad (3.2-15)$$

Substituting for the components of the current density in Equation 3.2-9 and expanding the resultant equation in the cylindrical coordinates yields the following working equations:

$$-\frac{\partial B_\phi}{\partial r} = \mu_o j_\theta = \mu B_\theta + \mu_o \frac{\partial p}{\partial r} \frac{B_\phi}{B^2}, \quad (3.2-16)$$

$$\frac{1}{r} \frac{\partial}{\partial r}(r B_\theta) = \mu_o j_\phi = \mu B_\phi - \mu_o \frac{\partial p}{\partial r} \frac{B_\theta}{B^2}. \quad (3.2-17)$$

These equations are derived based on a large aspect-ratio approximation. For a given μ and pressure profiles, these equations yield the components of the magnetic field. Usually values of poloidal beta, β_θ , toroidal plasma current, I_ϕ , and either reversal or pinch parameters are specified as the boundary conditions. The plasma-surface-averaged poloidal magnetic field, $\bar{B}_\theta(r_p)$, is approximated by

$$\bar{B}_\theta(r_p) = \frac{\mu_o I_\phi}{2\pi r_p}. \quad (3.2-18)$$

Except for special cases, such as the Bessel-function profiles, these equations must be integrated numerically (Section 5.2).

The plasma self-inductance, L_p , can be approximated by

$$L_p(H) = \mu_o R_T \left[\ln \left(\frac{8R_T}{r_p} \right) + \frac{l_i}{2} - 2.0 \right], \quad (3.2-19)$$

where $l_i \equiv \langle B_\theta^2 \rangle / \bar{B}_\theta^2(r_p)$ is the plasma internal inductance per unit length normalized to $\mu_o \equiv 4\pi \times 10^{-7}$ H/m. The vertical field, B_V , required to maintain the plasma toroidal equilibrium becomes [17]

$$B_V(T) = -\frac{\mu_o I_\phi}{4\pi R_T} \left[\ln \left(\frac{8R_T}{r_p} \right) + \beta_\theta + \frac{l_i}{2} - \frac{3}{2} \right], \quad (3.2-20)$$

which must be provided by the EF-coil pair (Section 4.6).

As implemented in the PSA code, the plasma inductance is expressed as a sum of an external inductance, $L_{p,ex}$, and an internal inductance, $L_{p,in}$ (*i.e.*, $L_p = L_{p,in} + L_{p,ex}$). The external inductance is taken to be that for a wire with the same dimensions as the plasma [18]:

$$L_{p,ex} = \mu_o R_T \left[\ln \left(\frac{8R_T}{r_p} \right) - 2.0 \right]. \quad (3.2-21)$$

The plasma internal inductance, as derived from results of the 1-D equilibrium calculation, is given by

$$L_{p,in} = \frac{1}{I_\phi^2} \left[2\pi R_T (W_\theta + W_\phi) - \frac{\Phi^2}{2L_o} \right], \quad (3.2-22)$$

where the internal magnetic energies, W_θ and W_ϕ , the toroidal magnetic flux, Φ , and the vacuum toroidal inductance, L_o , are given by

$$W_{\theta,\phi} \equiv \frac{\pi}{\mu_o} \int_0^{r_p} B_{\theta,\phi}^2(r) r dr, \quad (3.2-23)$$

$$\Phi \equiv 2\pi \int_0^{r_p} B_\phi(r) r dr, \quad (3.2-24)$$

$$L_o \equiv \frac{\mu_o r_p^2}{2R_T}. \quad (3.2-25)$$

Neglecting corrections for $Z_{eff} > 1$, the plasma pressure balance can be written in the approximate form

$$I_\phi = 2\pi r_p \left(\frac{2p}{\beta_\theta \mu_o} \right)^{1/2}, \quad (3.2-26)$$

where the average plasma pressure is $p \simeq 2nk_B T$ and k_B is the Boltzmann constant. The plasma line density is $N = n\pi r_p^2$ and the streaming parameter $\xi \equiv v_D/v_{THe} \propto I_\phi/N\sqrt{T_e}$, where $v_{THe} \equiv (2k_B T_e/m_e)^{1/2}$.

The PSA code searches for minimum-COE design points satisfying the steady-state burn condition, while balancing the plasma ohmic and fusion-product alpha power inputs against combined radiation and transport losses, such that

$$P_{OHM} + P_\alpha = P_{RAD} + P_{TR}, \quad (3.2-27)$$

at a profile-corrected Lawson parameter, $n\tau_E$, that is consistent with the stipulated plasma density and temperature profiles and the average plasma operating temperature, T [19]. The prompt alpha-particle loss to the first wall is expected to be negligible for typical RFP-reactor plasma currents of 15 to 20 MA.

The plasma ohmic power, P_{OHM} , is given by

$$P_{OHM} = g_{OHM} I_\phi^2 R_p = g_{OHM} \eta_{||} j_\phi^2 V_p, \quad (3.2-28)$$

where R_p is the plasma resistance and V_p is the plasma volume. The TITAN reactors operate with a highly radiating plasma. A fraction $f_{RAD} \equiv P_{RAD}/(P_{OHM} + P_\alpha) \simeq 0.95$

Table 3.2-III.
RFP ELECTRON ENERGY CONFINEMENT
SCALING PARAMETERS^(a)

ν	C_ν (s/m ² -MA ^{ν})
1.50	0.1400
1.40	0.1140
1.25	0.0837
1.20	0.0614
1.10	0.0620
1.05	0.0554
1.00	0.0500
0.90	0.0407
0.80	0.0331

(a) $\tau_E \equiv 2(1/\tau_{Ee} + 1/\tau_{Ei})^{-1}$,
 $\tau_{Ee} = C_\nu I_\phi^\nu r_p^2$; $\tau_{Ei} = 4\tau_{Ee}$.

of plasma power is radiated uniformly to the first wall to reduce the heat flux on the divertor-plate surfaces to a manageable level. Simultaneously, the plasma temperature and density in front of the divertor plate are reduced such that the sputtering of first-wall and divertor-plate structural surfaces is acceptable (Section 5).

The RFP electron energy confinement time, τ_{Ee} , is assumed to scale from values obtained in present-day experiments (Section 2.3.5) according to

$$\tau_{Ee}(PHYS) = C_\nu I_\phi^\nu r_p^2 f(\beta_\theta), \quad (3.2-29)$$

with typical values of the current scaling exponent, ν , and the corresponding numerical coefficient, C_ν , summarized in Table 3.2-III and Figure 2.3-20. The function $f(\beta_\theta)$ models the soft beta limit and is assumed to have a value of one for beta values below the beta limit and going to zero when the maximum beta value is exceeded.

The electrons lose energy by radiation and conduction (convection), while the ions lose energy only by conduction (convection). The total loss from the plasma, P , is

$$P = \frac{1.5n_i k_B T_i}{\tau_{Ei}} + \frac{1.5n_e k_B T_e}{\tau_{Ee}}, \quad (3.2-30)$$

where it is assumed that $\tau_{Ei} \simeq \tau_{ci} \simeq 4\tau_{Ee}$ is the ion energy confinement time and τ_{Ee} is the electron energy loss time given by Equation 3.2-29 above, which also includes the radiation losses (Section 5). For $n = n_i \simeq n_e$ and $T = T_i \simeq T_e$, and defining the plasma internal energy as $W_p = 3nk_B T$, the global plasma-energy loss rate can be rewritten as

$$P \equiv \frac{W_p}{\tau_E} = \frac{3n k_B T}{2} \left(\frac{1}{\tau_{Ei}} + \frac{1}{\tau_{Ee}} \right). \quad (3.2-31)$$

Therefore, the global energy confinement time, τ_E , is given by

$$\tau_E = 2 \left(\frac{1}{\tau_{Ei}} + \frac{1}{\tau_{Ee}} \right)^{-1}. \quad (3.2-32)$$

In the limit $\tau_{Ei} \rightarrow \infty$, $\tau_E = 2\tau_{Ee}$, and for $\tau_{Ei} = \tau_{Ee}$, $\tau_E = \tau_{Ee}$. A typical result for the TITAN design points is $\tau_E \simeq 0.2$ s.

The global energy confinement time of a minimum-COE design point, $\tau_E(OPT)$, at $P_E \simeq 1,000$ MWe as determined from the PSA code is typically consistent with $\nu \simeq 1.0$. Smaller output reactors with smaller values of r_p typically require $\nu > 1.0$ (*i.e.*, better intrinsic energy confinement). The effective global diffusivity is defined for parabolic temperature and flat density profiles such that $\chi_E = (3/16)r_p^2/\tau_E$. The confinement time parameter space for the TITAN-I reference design is illustrated in Figure 3.2-2. A viable design requires $\tau_E(ECON) < \tau_E(PHYS)$, so that only a sufficiently high value of ν is of interest.

In steady state, the fusion alpha-particle confinement time, $\tau_{p\alpha}$, is defined by

$$\dot{n}_\alpha = 0.25 g_{DT} n_i^2 \langle \sigma v \rangle_{DT} - \frac{n_\alpha}{\tau_{p\alpha}} = 0, \quad (3.2-33)$$

The impurity control and particle exhaust system should be designed to have adequate pumping efficiency to remove the alpha ash. The fuel-ion fractional burnup, f_B , is given by

$$f_B = \left(1 + \frac{2}{g_{DT} n_i \langle \sigma v \rangle_{DT} \tau_{pi}} \right)^{-1}. \quad (3.2-34)$$

A typical result for a TITAN design point is $f_B \simeq 0.06$.

The PSA code couples the above-described physics model with engineering and models described in the following subsections. Elaboration of the physics basis and related issues of the TITAN study is found in Sections 2 and 4 through 8.

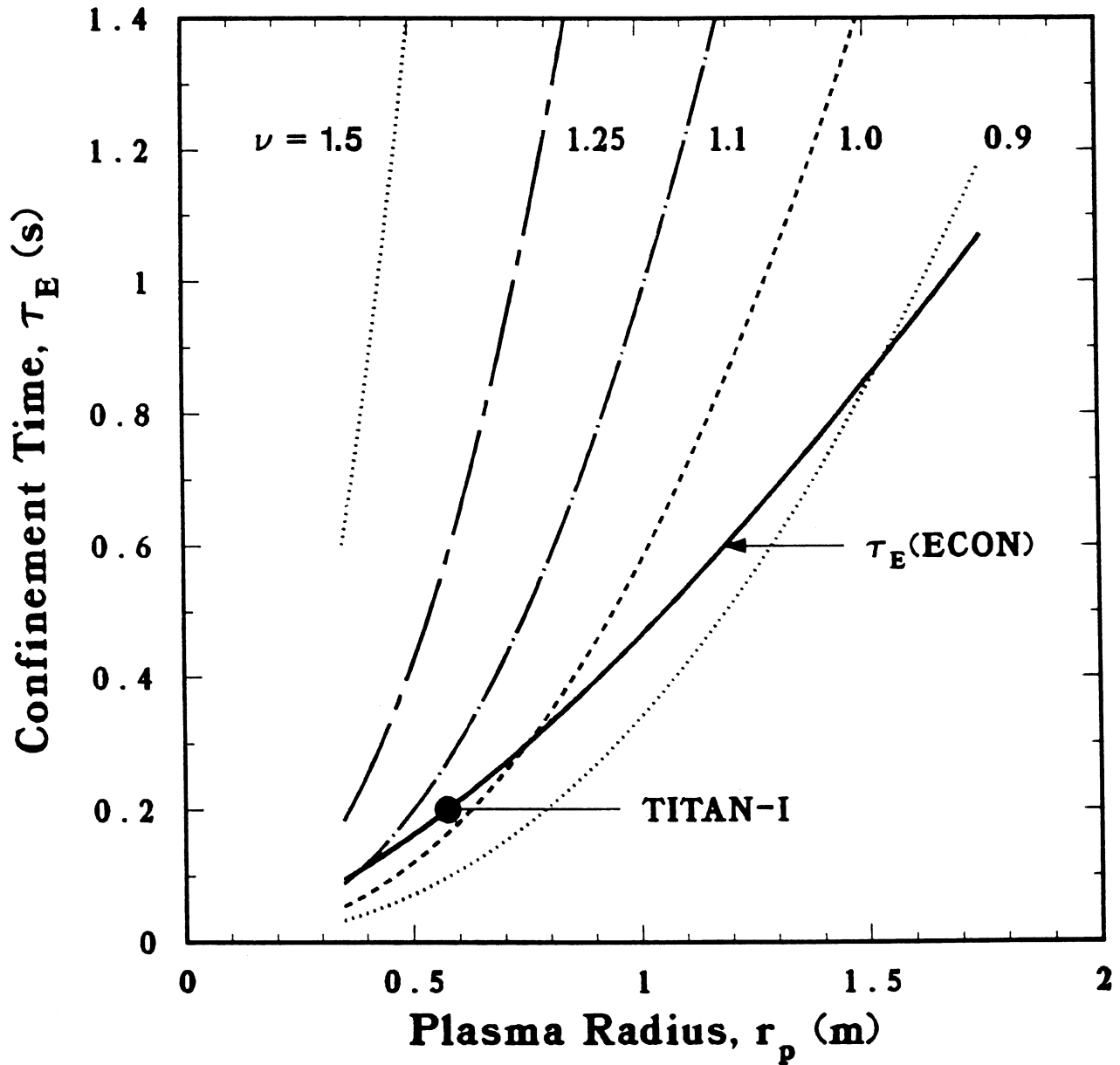


Figure 3.2-2. Comparison of the dependence of the global energy confinement time on plasma minor radius for various values of the plasma-current scaling exponent, ν . The economic confinement time, $\tau_E(\text{ECON})$, for TITAN-class reactors is also shown as a function of r_p . The TITAN-I reference design point is denoted by the filled circle.

3.2.2. Reactor Engineering Model

Given a stipulated target for the net electric-power output, P_E , the thermal-power output, P_{TH} , is determined for a nominal value of the thermal conversion efficiency, η_{TH} , such that $P_E = \eta_{TH}(1 - \epsilon)P_{TH}$, where $\epsilon = 1/Q_E$ is the recirculating power fraction. The gross electric-power output is $P_{ET} = \eta_{TH}P_{TH}$. A fraction f_{AUX} of P_{ET} is allocated for auxiliary functions, such that $P_{AUX} = f_{AUX}P_{ET}$. A fraction f_{pump} of P_{ET} is allocated for primary-coolant pumping power, such that $P_{pump} = f_{pump}P_{ET}$. Of this latter contribution to the recirculating power, it is assumed that $0.85P_{pump}$ is recoverable as useful thermal power in the primary loop. The plasma ohmic-heating power, P_{OHM} , joule dissipation in the respective resistive coil sets, P_{TF}^Ω and P_{DF}^Ω , and current-drive power, P_{CD} (including P_{OHM}) complete the components of recirculating power for the TITAN. Power dissipation attributable to OFCD in the various coil sets and in the first wall, blanket, and shield is calibrated by separate calculations (Section 7). If the EF coil is taken to be superconducting, $P_{EF}^\Omega = 0$. Additionally, following the start-up transient, the OH-coil current would be slowly ramped to zero, such that for purposes of the average steady-state power balance, $P_{OH}^\Omega = 0$.

The engineering Q-value figure of merit, Q_E , can be written as

$$Q_E = \frac{1}{\epsilon} = \eta_{TH} \frac{M_N P_N + P_\alpha + P_{OHM} + 0.85P_{pump} + P_{IBC}^\Omega}{P_{AUX} + P_{pump} + P_{TF}^\Omega + P_{DF}^\Omega + P_{CD}}, \quad (3.2-35)$$

where M_N is the blanket neutron energy multiplication ratio and is found from neutronics calculations to be 1.2 for the TITAN-I design (Section 10.3) and 1.36 for the TITAN-II design (Section 16.3). For the TITAN-I design with the IBC option [13], the dissipated power, P_{IBC}^Ω , in the resistive TF and divertor IBCs is also included in the useful thermal power, P_{TH} .

The average 14.1-MeV neutron first-wall load, I_w , is given by

$$I_w = \frac{14.06}{17.58} \frac{P_F x}{4\pi^2 A r_p^2}, \quad (3.2-36)$$

where P_F is the DT fusion power and $x \equiv r_p/r_w$ is the plasma filling fraction. A nominally constant scrape-off layer thickness is presently assumed such that $r_w = r_p + 0.06$ m for TITAN designs. The ratio of the first-wall radius to the plasma radius is $r_w/r_p \simeq 1.1$ at the TITAN reference design points. The dependence of I_w on r_p for TITAN-I is illustrated in Figure 3.2-3. For these reactors, the various components of Q_E included in Equation 3.2-35 adjust among themselves so that Q_E itself is quite insensitive to FPC size, as is also illustrated in Figure 3.2-3.

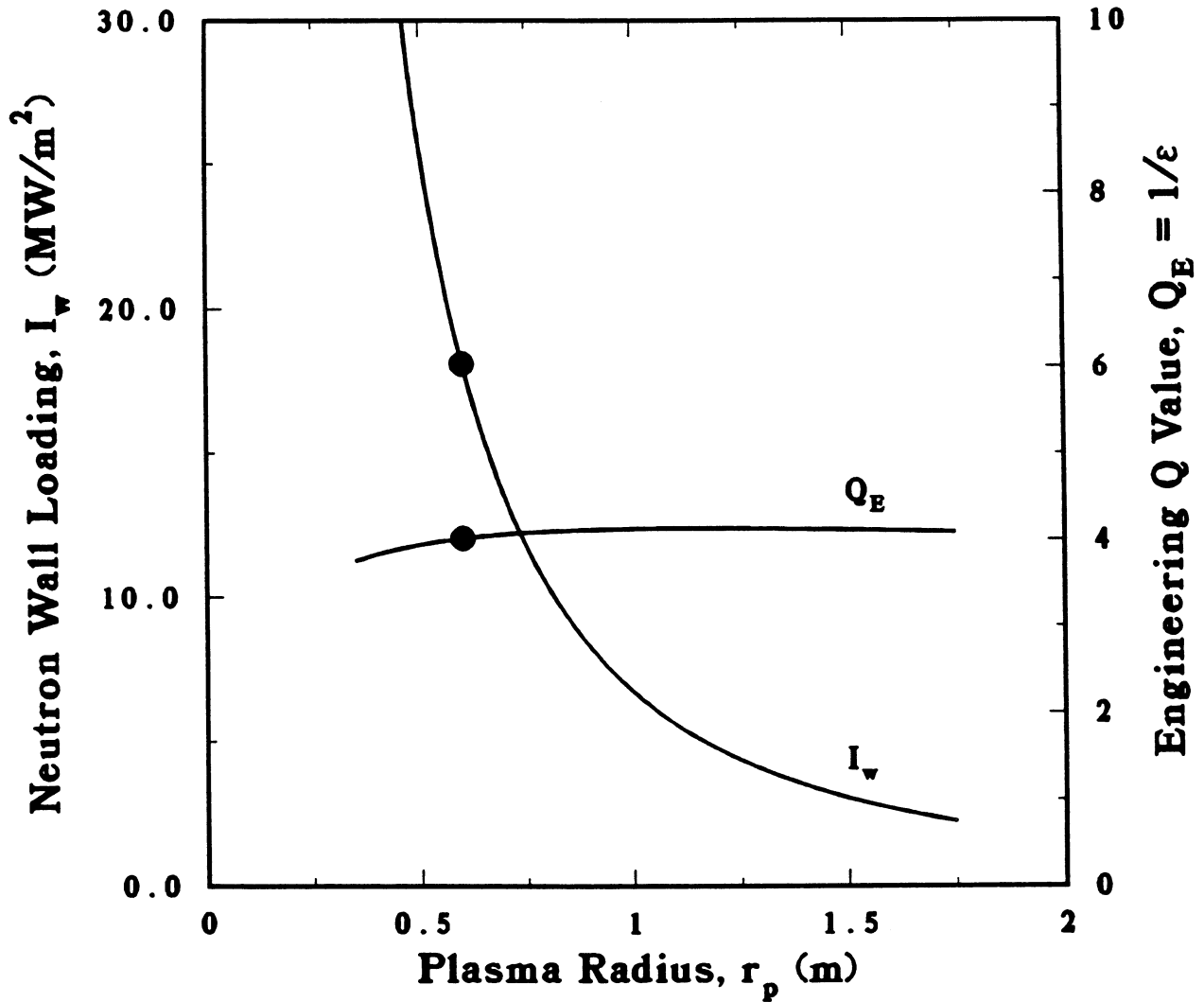


Figure 3.2-3. Dependence of the neutron wall loading and the engineering Q-value on plasma minor radius for the TITAN-I-class reactors. The TITAN-I reference design point is denoted by the filled circle.

The resistivity of the copper coil is taken to be $\rho_{Cu} = 2.0 \times 10^{-8} \Omega\text{m}$ at the coil operating temperature $\sim 20^\circ\text{C}$. Typically, the effective resistivity is increased by $1/\lambda_c$, where $\lambda_c \simeq 0.7$ is the assumed conductor filling fraction, pending a more detailed design of the coil internals. The mass density of the copper coils is consistent with a composition of 10% coolant, 10% structure, and 10% insulator (all by volume). A similar assumption applies to the superconducting EF coils resulting in a effective coil mass density of $\rho_c \simeq 7300 \text{ kg/m}^3$. For superconducting EF coils, the maximum coil current density is given by [20]

$$j_m(\text{MA/m}^2) = \frac{96 - B_{\theta c}}{1 + (B_{\theta c}/12)^{1.5}}, \quad (3.2-37)$$

where $B_{\theta c}$ is the local magnetic-field strength, in units of tesla, calculated at the EF-coil surface.

The OH-coil set is sized by applying the start-up flux-swing condition,

$$L_p I_\phi (1 + f_{RES}) = M_{EF,p} I_{EF} + M_{OH,p} \Delta I_{OH}, \quad (3.2-38)$$

where $M_{EF,p}$ is the mutual inductance between the EF-coil set and the plasma, $M_{OH,p}$ is the mutual inductance between the OH-coil set and the plasma, $\Delta I_{OH} \equiv I_{OH}^+ - I_{OH}^-$ is the change (swing) during the start-up rise time, τ_R , of the OH-coil current from its initial (back-bias) value I_{OH}^- to its value at full plasma current, I_{OH}^+ . After the OFCD system is fully operational, the OH current is slowly ramped down to zero. The factor

$$f_{RES} \simeq 2 g_{OHM} \frac{R_p}{L_p} \tau_R, \quad (3.2-39)$$

provides for resistive flux dissipation in the plasma during the start-up transient. The parameter $f_G \equiv I_{OH}^+ / |I_{OH}^-|$ is used to characterize the symmetry of the bipolar current swing and $f_G = 1$ achieves a symmetric OH-coil current swing. Smaller values of f_G represent deeper initial back-bias current (*i.e.*, larger I_{OH}^-) and result in higher values of OH-coil stress at back bias.

Both resistive and inductive factors contribute to the power supply requirements and cost of the separate OH and EF-coil sets according to

$$P_c = I_c^2 R_c \left(1 + \frac{L_c/R_c}{\tau_R} \frac{\Delta I_c}{I_c} \right), \quad (3.2-40)$$

where subscript c denotes either OH or EF coils. The two-stage ramp-up of the TITAN RFP draws power from the grid only during the slow second stage (~ 8 to 15 s) which follows the discharge of the stored magnetic energy in the OH-coil set during the first-stage,

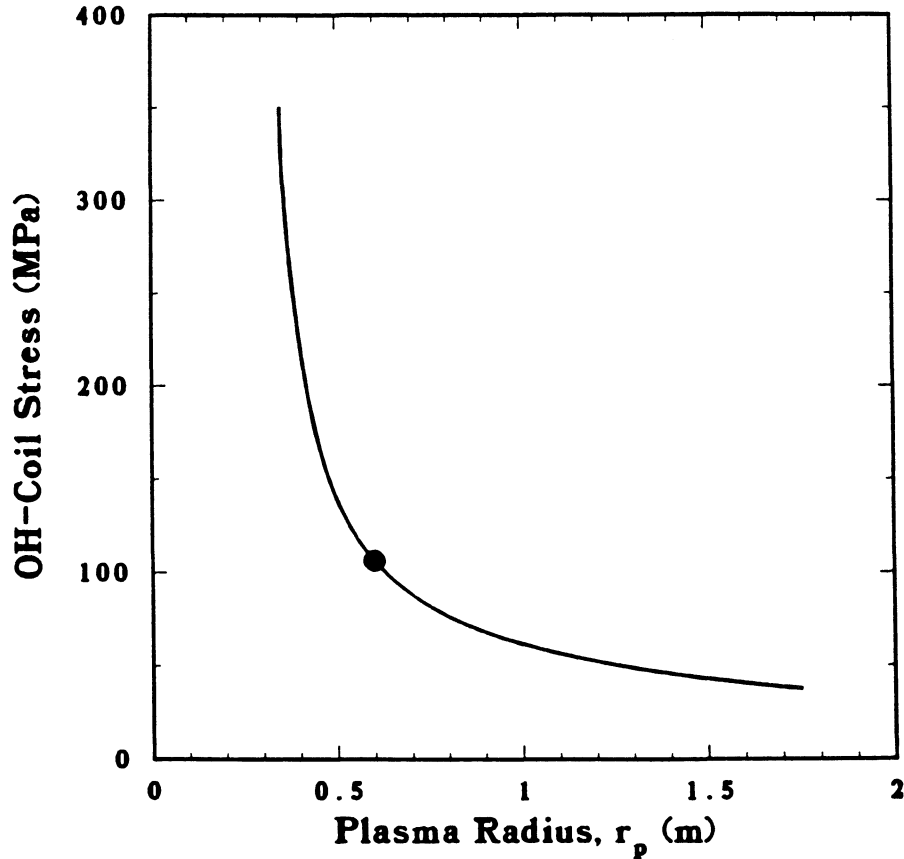


Figure 3.2-4. Dependence of back-bias OH-coil von Mises stress at $f_G \equiv I_{OH}^-/I_{OH}^+ = 1.0$ on plasma minor radius. The TITAN-I reference design is denoted by a filled circle. The stress for $f_G = 0.2$ approaches the nominal design limit of 200 MPa.

fast-ramp phase (1 to 2 s). Therefore, the PSA code approximates $\Delta I_{OH} \simeq (I_{OH}^+ + 3)$ MA and $\Delta I_{EF} \simeq (I_{EF}^+ - 13)$ MA for purposes of Equation 3.2-40. A more detailed start-up simulation is considered in Section 6.2.

The OH-coil stresses are estimated approximately using a von Mises stress [21] given by

$$\sigma_{OH} = (\sigma_r^2 + \sigma_\theta^2 - 2\nu_{OH}\sigma_r\sigma_\theta)^{1/2}, \quad (3.2-41)$$

where σ_r and σ_θ are the respective radial and loop stress components and $\nu_{OH} \simeq 0.3$ is the effective OH-coil Poisson ratio. A maximum upper limit to OH-coil stress evaluated at the back-bias condition is taken to be $\sigma_{OH} \leq 200$ MPa. The dependence of σ_{OH} on r_p for TITAN-I is illustrated in Figure 3.2-4.

TITAN reactors operate at steady state using an OFCD system to maintain the plasma current (Section 7). Factors calibrating the AC joule dissipation in the first wall, blanket, shield, and coils have been calculated separately and incorporated into the PSA model. The efficiency of the OFCD power supply is monitored by means of a circuit Q-value, $Q_{PS} \simeq 100$. The P_{CD} term in Equation 3.2-35 represents the sum of these losses.

Drained blanket, shield, and coil masses are calculated using homogenized densities. The FPC mass, M_{FPC} , is used to compute mass utilization M_{FPC}/P_{TH} (tonne/MWt) and mass power density, MPD (kWe/tonne), figures of merit (Reference [22] and Appendix C of Reference [5]). These figures of merit have been found to be useful, but not rigorous, predictors of cost trends. Minimum-COE TITAN design points occur for MPD $\simeq 800$ kWe/tonne.

The small physical size and mass of high MPD reactors makes a single-piece maintenance procedure feasible. In this scheme, the entire reactor torus is replaced as a single unit. Single-piece maintenance is expected to have a strong influence on the plant availability. System redundancy, steady-state operation, ease of reactor torus replacement, and development of reliable components should permit the nominal overall plant availability of $p_f \simeq 76\%$ for the TITAN designs. Steady-state operation should also considerably improve reliability for the application of economically optimum engineering safety factors. The plant availability is reduced from 100% because of the outage time for unscheduled maintenance, t_u , and scheduled maintenance, t_s (days per year),

$$p_f = 1 - \frac{t_u + t_s}{365}. \quad (3.2-42)$$

The scheduled outage time, t_s , is the maximum of the outage time for the maintenance of the balance of plant, t_{so} , and the maintenance of the FPC, $t_s^{FPC} = \tau_s/t$, where τ_s is the reactor-torus replacement time (in days) and $t = (I_w\tau)/(I_w p_f)$ is the operational lifetime of the FPC (in years) which is limited by the fluence lifetime of the first wall, $I_w\tau$.

To achieve the target availability, the unscheduled outage time, t_u , is set at 60 days per year, the scheduled maintenance of the balance of plant, t_{so} is set at 28 days per year, it is assumed that scheduled maintenance of the FPC requires $\tau_s = 28$ days per reactor-torus replacement, and a typical first-wall fluence lifetime of $I_w\tau = 15$ MWy/m² is used. For a plant availability of 76%, the operational lifetime is one year at $I_w \simeq 20$ MW/m². For lower wall loads, the lifetime of the FPC is longer than one year and the FPC can be replaced during the scheduled maintenance time of the balance of plant. Then, the scheduled outage time, $t_s = t_{so} = 28$ days per year and the plant availability remains at 76% and independent of I_w .

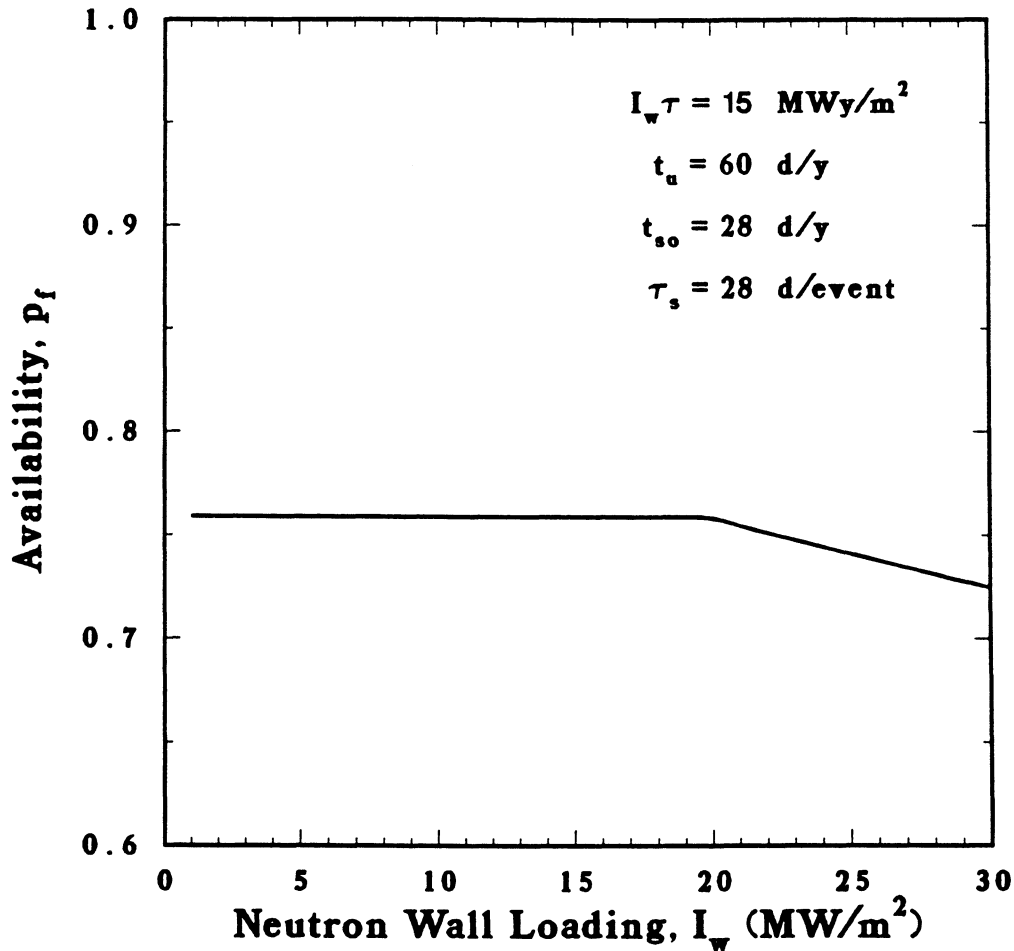


Figure 3.2-5. TITAN plant availability, p_f , as a function of neutron first-wall load, I_w , for the indicated nominal parameters. At very high I_w , the FPC change-out rate becomes large such that p_f is penalized.

For wall loads higher than 20 MW/m^2 , the operational lifetime of the FPC is less than one year and the scheduled outage time is $t_s = t_s^{FPC} = \tau_s/t$, which results in a decrease in the plant availability factor for high I_w . This dependence of p_f on I_w is expressed by

$$p_f = \begin{cases} \frac{365 - t_u - t_{so}}{365} = 0.76 & \text{for } \frac{I_w}{(I_w \tau)} < \frac{1}{0.76} \text{ y}^{-1} \\ \frac{365 - t_u}{365 + (I_w \tau_s)/(I_w \tau)} & \text{for } \frac{I_w}{(I_w \tau)} > \frac{1}{0.76} \text{ y}^{-1} \end{cases} \quad (3.2-43)$$

and is illustrated in Figure 3.2-5. For wall loads such that $I_w \leq (I_w \tau)/p_f$, the annual change-out of the FPC is assumed such that $p_f \simeq 0.76$. As I_w exceeds $I_w \tau/p_f$, the FPC

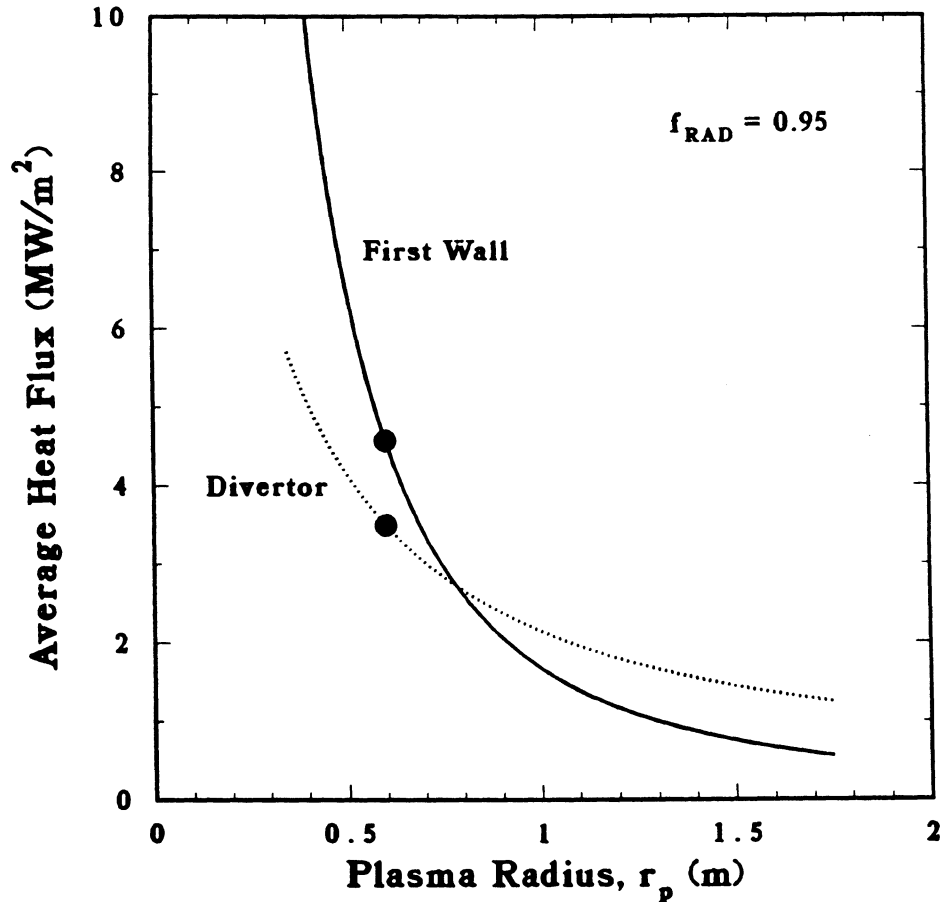


Figure 3.2-6. Dependence of first-wall and divertor-plate surface heat loads on plasma minor radius for a radiation fraction of $f_{RAD} = 0.95$. The TITAN-I reference design point is denoted by a filled circle.

change-out rate is accelerated and p_f is penalized as is shown. It is seen that at very high wall loads, the periodic first-wall and blanket replacement becomes an important operational feature.

A high-power-density RFP reactor must operate with a highly radiating plasma to distribute the plasma energy uniformly on the first wall and reduce the heat flux on the divertor plates to a manageable level. The TITAN plasma radiates a considerable fraction, $f_{RAD} \simeq 0.95$, of the combined plasma power, $P_\alpha + P_{OHM}$ (70% radiation from the core and additional 25% from the scrape-off layer). Assuming three divertors with area $A_{DIV} \simeq 7 \text{ m}^2$ (Section 11), the average surface heat load for TITAN-I design is illustrated in Figure 3.2-6.

3.3. COSTING

The estimated cost of electricity (COE) is the most important evaluation tool to optimize and compare with alternative energy sources. The estimated COE is the object function of the PSA code. Both constant-1986 and then-current-1992 dollar analyses are used to evaluate the TITAN economic parameters for an assumed six years construction time. The general equation for bus-bar energy cost is given by

$$COE = \frac{C_{AC} + (C_{O\&M} + C_{SCR} + C_F)(1 + y)^Y}{8760 P_E p_f}, \quad (3.3-1)$$

where

COE	Cost of electricity in constant or then-current dollars (mill/kWh),
C_{AC}	Annual capital cost charge, equals the "overnight" total capital cost (TCC) multiplied by the fixed charge rate (FCR),
C_i	Cost of account i ,
$C_{O\&M}$	Annual operations and maintenance (O&M) cost, $C_{40} + C_{41} + \dots + C_{47}$,
C_{SCR}	Annual scheduled component replacement (SCR) cost, $C_{50} + C_{51}$,
C_F	Annual fuel costs, C_{02} and C_{03} ,
y	Annual escalation rate,
Y	Construction period (year),
P_E	Net plant electric-power output (MWe),
p_f	Plant availability factor,
TDC	Total direct cost = $\sum_{i=20}^{26} C_i$,
C_{IDC}	Interest during construction, $C_{97} = f_{IDC}$ TDC,
C_{EDC}	Escalation during construction $C_{98} = f_{EDC}$ TDC,
TCC	Total capital cost = $\sum_{i=20}^{98} C_i$.

The detailed methodology for calculating the TITAN time-related cost factors is described in References [20] and [23] and will not be repeated here. This description differs from the U. S. fusion-reactor-community standards [24 - 26] used in the period 1980-1985 because of a slightly-different "s-shaped" spending profile assumed, but represents the pending standard for U. S. fusion-reactor studies for the foreseeable future [27]. Fixed charge rate (FCR) values are summarized in Table 3.3-I. The reference TITAN case assumed an annual inflation/escalation rate, $y = 0.06/y$, to give, under the standard assumptions [23] an annual utility cost of money (COM) of $x = 0.09/y$, a constant-dollar-mode levelized annual fixed charge rate (LAFCR) of $0.08/y$, and a corresponding

then-current-dollar-mode LAFCR of 0.136/y. Factors used to obtain interest-during-construction (IDC) and escalation-during-construction (EDC) costs are summarized in Table 3.3-II. The TITAN study uses the upper set of factors, consistent with $y = 0.06/y$ and $x = 0.09/y$. The lower set, assuming $y = 0.05/y$ and $x = 0.10/y$, is characteristic of the older U. S. fusion-community standard [23 - 25]. Differences between the standards are not large.

The direct cost account entries, C_i , are obtained by applying relevant (installed) unit-cost estimates (*e.g.*, \$/W, \$/kg, \$/m³), where known, to the calculated usage of these items in the conceptual design, such that $C_i(\$) = u_i(\$/\text{unit})X_i(\text{unit})$. A learning-curve or

Table 3.3-I.
EFFECTIVE COST OF MONEY (COM) AND
LEVELIZED ANNUAL FIXED CHARGE RATE (LAFCR)^(a)

Escalation Rate, y (%/y)	COM, x (%/y)	LAFCR (%/y)
0	4.2	8.0 ^(b) (10.0) ^(c,d)
2	5.8	9.7
4	7.4	11.6
5	NA	NA (15.0) ^(d)
6 ^(b,e)	9.0 ^(b,e)	13.6 ^(e) (16.5) ^(c)
8	10.6	15.8
10	12.2	18.1

(a) Reference [23].

(b) TITAN reference case for constant-dollar mode.

(c) Reference [20].

(d) Reference [24].

(e) TITAN reference case for then-current-dollar mode.

Table 3.3-II.
**TIME-RELATED COST FACTORS^(a) AS FUNCTIONS OF
 CONSTRUCTION LEAD TIME**

Lead Time, Y (y)	Capitalization Factors		Interest Factor
	f'_{cap} (current-dollar)	f'_{cap0} (constant-dollar)	f'_{IDC}
For $y = 0.06/y$ and $x = 0.09/y$:^(b)			
1	0.0788	0.0177	0.0556
2	0.1558	0.0287	0.0908
3	0.2386	0.0399	0.1274
4	0.3273	0.0513	0.1652
5	0.4224	0.0629	0.2042
6 ^(c)	0.5244	0.0747	0.2444
7	0.6338	0.0866	0.2858
8	0.7511	0.0986	0.3284
9	0.8768	0.1109	0.3723
10	1.0117	0.1233	0.4176
For $y = 0.05/y$ and $x = 0.10/y$:			
1	0.0812	0.0297	0.0617
2	0.1558	0.0484	0.1011
3	0.2359	0.0676	0.1424
4	0.3217	0.0873	0.1853
5	0.4135	0.1076	0.2299
6	0.5120 ^(d)	0.1282 ^(d)	0.2761 ^(d)
7	0.6174	0.1494	0.3240
8	0.7303	0.1711	0.3738
9	0.8512	0.1933	0.4254
10	0.9808	0.2161	0.4790

(a) $f_j \equiv 1 + f'_j$.

(b) *cf.* Table D.I, p. 237, Reference [20].

(c) TITAN reference case for $Y = 6$ y construction time.

(d) *cf.* Reference [24]:

$$f'_{CAP} \equiv (F_{IDC} + F_{EDC}) = (0.316 + 0.190) = 0.506, f'_{cap0} = 0.129, f'_{IDC} = 0.316.$$

mass-production credit is taken for a “tenth-of-a-kind” commercial reactor installation, consistent with U. S. fusion-reactor-design-community practice. Often, the cost data base consists of cost-scaling relationships of the form

$$C_j(\$) = c_j(X_j)^{e_j}, \quad (3.3-2)$$

where X can be either a descriptive variable (*e.g.*, power, mass, volume) or a scaled variable, X_k/X_{REF} , related to a reference value, X_{REF} of X_j , and e_j is an appropriate scaling exponent (usually $0 < e_j < 1$). Equation 3.3-2 can be rewritten in the form

$$C_j(\$) = \frac{c_j(X_j)^{1-e_j} (X_j)^{e_j}}{(X_j)^{1-e_j}} = \left[\frac{c_j}{(X_j)^{1-e_j}} \right] X_j, \quad (3.3-3)$$

which allows the definition of a (variable) unit cost

$$u_j = \left[\frac{c_j}{(X_j)^{1-e_j}} \right], \quad (3.3-4)$$

which is a dependent function of the descriptive variable, X_j , itself. While the cost accounting scheme allows for detailed cost breakdowns (to four levels), only a relatively sparse, but comprehensive, subset of items are estimated reported explicitly. The cost scaling exponents, e_j , used in the TITAN study are typically consistent with those of the U. S. nuclear-fission-reactor experience [28] and represent the inclusion of quality-control costs associated with nuclear-grade (“N-stamped”) components. Potential cost savings derived from the substitution of conventional (non-nuclear) components under the condition of demonstrable inherent safety (Sections 13 and 19) are significant [29,30] but controversial [31]. These savings (up to 25% on selected items) have not been included in the TITAN data base. The essential elements of the TITAN cost data base [2,5] are summarized in Table 3.3-III. Costs which date from sources using a 1980-dollar reporting base are scaled to a 1986 reporting base using the multiplicative factor 1.348 [5].

For purposes of costing in the PSA code, the reactor building is divided into a variable-volume reactor cell, housing the FPC and vacuum tank, and a fixed-volume region, housing the primary heat-transport loops. The volume of the latter portion is estimated to be $1.55 \times 10^5 \text{ m}^3$ and is similar to that of the STARFIRE [32] design after escalating costs. The reactor room is modeled by a rectilinear enclosure extending horizontally 9 m beyond the FPC with a height approximately three times that of the FPC, such that $V_{RB} (\text{m}^3) = 16(R_T + r_s + 9)^2 (6r_s) + 1.55 \times 10^5$. The basic building structure (Account 21.2.1) is priced at 300 m^3 , a value between that of STARFIRE [32] and MARS [33] designs. To this value, 2 M\$ is added for building services (Account 21.2.2),

Table 3.3-III.
SUMMARY OF TITAN COST DATA BASE^(a,b)

Acct. No.	Account Title	Cost (M\$, 1980 ^(c))
20.	Land and Land Rights	3.3
21.	Structures and Site Facilities	
21.1	Site improvements and facilities	11.28
21.2	Reactor building	$3.0 \times 10^{-4} V_{RB} + 39.5$
21.3	Turbine building	33.5
21.4	Cooling structures	$7.135 (P_{ET}/1000)^{0.3}$
21.5	Power supply and energy storage bldg.	9.16
21.6	Miscellaneous buildings	76.5
21.7	Ventilation stack	1.81
22.	Reactor Plant Equipment (RPE)	
22.1	Reactor equipment	
22.1.1.1	Breeding material:	
	Liquid metal (LM): PbLi ^(d,e)	(see Acct. no. 26.1)
	Li ^(d,f)	(see Acct. no. 26.1)
	Water solution: LiNO ₃ ^(d,g)	$(7.83 f_{6Li} + 2.46) \times 10^{-3} M$
22.1.1.2	Blanket and first-wall structure	$0.0533 M_{BL}$
22.1.1.3	Be multiplier ^(g)	$0.3338 M_{Be}$
22.1.2	Shield:	
	V alloy ^(f)	$0.1855 M_{SHD}$
	Ferritic steel ^(g)	$0.0157 M_{SHD}$
22.1.3	Magnet coils:	
	Normal conducting	$0.065 M_c$
	Superconducting	$0.130 M_c$
22.1.4	Supplemental (RF) heating systems ^(h)	$1.65 P_{RF}$
22.1.5	Primary structure and support	$0.1125 V_{STR}$
22.1.6	Reactor vacuum system	$0.015 M_{VAC}^{(f)} + 2.5 \text{ (kg/d)}$

Table 3.3-III (Cont'd)

Acct. No.	Account Title	Cost (M\$, 1980 ^(c))
22.1.7	Power supply (switching, energy storage):	
	Normal-conducting coils	18.55 \$/kVA
	Superconducting coils	296.7 \$(kVA) ^{0.8}
	IBC ^(f)	37.09 \$/kVA
	OFCO	37.09 \$/kVA
	Other	1.0
	TF IBC busbars ^(f)	3.034
	DF IBC busbars ^(f)	1.625
22.1.8	Impurity control system	0.66 A_{DIV}
22.1.9	Direct energy conversion ^(h)	0.0
22.1.10	ECRH breakdown system	1.589
22.2	Main heat-transfer system	
22.2.1	Primary coolant:	
	Li ^(f)	$u_j = 0.2013 [P_{TH}(1 - f_w)]^{-0.2} (i)$ $X_j = P_{TH}(1 - f_w)$
	H ₂ O ^(g)	$u_j = 0.1030 [P_{TH}(1 - f_w)]^{-0.2} (i)$ $X_j = P_{TH}(1 - f_w)$
22.2.2	Intermediate-coolant system	$u_j = 0.1030 P_{TH}^{-0.2} (i)$ $X_j = P_{TH}$
22.2.3	Secondary-coolant system	$u_j = 0.1030 (P_{TH} f_w)^{-0.2} (j,e)$ $X_j = P_{TH} f_w$
22.3	Auxiliary cooling systems	$6.7 \times 10^{-4} P_{TH}$
22.4	Radioactive-waste treatment	$1.2 \times 10^{-3} P_{TH}$
22.5	Fuel handling and storage	
22.5.1	Pellet injectors	3.709 M\$ each $\times 2 (f,g,i)$
22.5.2	Fuel processing system	0.5 (g/day) ^{0.7}
22.5.3	Fuel storage	3.709
22.5.4	Atmospheric tritium recovery	0.2 (m ³ /h) ^{0.6}
22.5.5	Water-detrutiation system:	
	TITAN-I	5
	TITAN-II	140

Table 3.3-III (Cont'd)

Acct. No.	Account Title	Cost (M\$, 1980 ^(c))
22.6	Other reactor plant equipment	$1.09 \times 10^{-3} P_{TH}$
22.7	Instrumentation and control	23.41
23.	Turbine Plant Equipment	
23.1	Turbine generators	$59.9 (P_{ET}/1000)^{0.7}$
23.2	Main steam system	$4.80 (P_{TH}/2860)$
23.3	Heat rejection systems	$0.0632 (P_{TH} - P_{ET})^{0.8}$
23.4	Condensing system	$13.8 (P_{ET}/1000)^{0.9}$
23.5	Feed heating system	$7.55 (P_{TH}/2860)$
23.6	Other turbine plant equipment	$40.9 (P_{ET}/1000)^{0.6}$
23.7	Instrumentation and control	$7.8 (P_{ET}/1000)^{0.3}$
24.	Electric Plant Equipment	
24.1	Switchgear	$8.6 (P_{ET}/1000)$
24.2	Station service equipment	$14.2 (P_{ET}/1000)$
24.3	Switchboards	$5.4 (P_{ET}/1000)$
24.4	Protective equipment	2.11
24.5	Electrical structures and wiring containers	$11.12 + 6.28 (P_{ET}/1440)$
24.6	Power and control wiring	$23.0 + 13.0 (P_{ET}/1440)$
24.7	Electrical lighting	8.2
25.	Miscellaneous Plant Equipment	
25.1	Transportation and lifting equipment	15.68
25.2	Air and water service systems	12.35
25.3	Communications equipment	6.22
25.4	Furnishings and fixtures	1.20
26.	Special Materials	
26.1	Reactor LM coolant/breeder ^(d)	
	PbLi ^(e)	$(7.83 f_{eLi} + 2.46) \times 10^{-3} M_{LM}$
	Li ^(f)	$(1169 f_{eLi} + 58.0) \times 10^{-3} M_{LM}$
26.4	Other	0.25
26.5	Reactor-building cover gas (Argon) ^(f)	0.13

Table 3.3-III (Cont'd)

Acct. No.	Account Title	Cost (M\$, 1980 ^(c))
90.	Total Direct Cost (TDC)	
91.	Construction Services and Equipment (10% of TDC)	
92.	Home-Office Engineering and Services (10% of TDC)	
93.	Field-Office Engineering and Services (10% of TDC)	
94.	Owner's Cost (5% of TDC)	
95.	Process Contingency (5% of TDC) ^(h)	
96.	Project Contingency (10% of TDC)	
97.	Interest during Construction (IDC)	
98.	Escalation during Construction (EDC)	
99.	Total Capital Cost (TCC)	

(a) Gross electric power, P_{ET} , net electric power, P_E , and total thermal power, P_{TH} , are given in MW. Volumetric V (m³) or corresponding mass M (tonne) unit costs for the fusion power core (FPC) and related items are given as follows:

Reactor building, $V_{RB} = 4(R_T + r_s + 9)^2(6r_s) + 1.55 \times 10^5$ (m³),

Blanket structure (5%), M_{BL} (tonne), Shield, M_{SHD} (tonne),

Magnet coils, M_C (tonne), Structure, V_{STR} (m³),

Vacuum tank, $M_{VAC} = (0.07)(7.8)2\pi[(R_T + r_s + 3)^2 + 4r_s(R + r_s + 3)]$ (tonne),

Divertor-plate surface area, A_{DIV} (m²).

(b) Refer to Appendices A and B for detailed TITAN design cost summaries.

(c) 1980 costs are multiplied by 1.348 to yield 1986 costs.

(d) Liquid metal, M_{LM} (tonne): ⁶Li enriched, $0.075 < f_{6Li} < 0.90$.

(e) Applicable to CRFPR.

(f) Applicable to TITAN-I.

(g) Applicable to TITAN-II.

(h) Not applicable to TITAN.

(i) cf. Equation 3.3-4.

40 M\$ for containment structures (Account 21.2.3), and 10.1 M\$ for architectural costs (Account 21.2.4). The TITAN FPC is represented by most of the Reactor Equipment (Account 21.1) items. Supplemental-RF-heating system (Account 22.1.4) and direct-energy-conversion system (Account 22.1.9) are not applicable to the TITAN design. On a unit-cost basis, superconducting-coil power supplies are considerably more expensive than resistive-coil power supplies. Power supplies for IBC and associated electrical bussing are more expensive than power supplies for conventional multi-turn resistive coils.

The main heat-transfer system for TITAN-I includes a liquid-metal primary loop serving the blanket, divertor, and shield. Allowances are made for a fraction, f_w , of thermal power to be delivered to a pressurized-water loop. The cost of the liquid-metal loop (Account 22.2.1) calibrated by the dual-media (PbLi and water) MARS design [33] with a reduction of 80% of the dominant piping costs of that design to reflect the shorter pipe runs in the TITAN case. This model results in an ~ 50 M\$ increase in cost over the pressurized-water main heat-transfer system in STARFIRE [32]. In the TITAN-I case, where Li is the sole primary coolant, f_w is zero; in the TITAN-II case, f_w is one. The liquid-metal inventory in the system consists of 95% of the blanket volume, corrected by a factor of 1.09 to account for the FPC ducts connecting the blanket through the magnet sets to the main manifolds. To this variable volume is added a fixed increment ($\sim 500 \text{ m}^3$) for the primary-loop inventory, a value assumed to be relatively constant over the parameter range of interest. The cost of the liquid metal in the primary loop is reported under Special Material (Account 26), insofar as it is salvageable and reusable. The unit cost of the liquid metal (PbLi or Li) is a linearly increasing function of the ${}^6\text{Li}$ enrichment, $f_{{}^6\text{Li}}$, as shown on Figure XIV.3-1 of Reference [34].

The reactor-torus replacement-cost estimate applies a factor of two to the direct cost of these components to allow for the handling and replacement of the spent reactor torus. For an assumed first-wall fluence life, $I_w\tau = 15 \text{ MWy/m}^2$ at a cost-optimized neutron wall loading of $I_w \simeq 20 \text{ MW/m}^2$ and a plant factor $p_f \simeq 0.76$, routine FPC replacement occurs annually. Account 50 represents $\sim 9\%$ of the basecase COE for TITAN-I and $\sim 3\%$ for TITAN-II, and is distinct from the nominal annual operations and maintenance (O&M) charge (Accounts 40-47, 51), conservatively estimated [24,25] to be 2% of the direct cost. This scheme costs the first reactor, first wall, and blanket twice, and credit is not taken for any reuse of reactor-torus components (*i.e.*, TITAN-II TF coils or shield).

3.4. TITAN-I DESIGN POINT

3.4.1. Design Point Selection

The Los Alamos CRFPR framework studies [2,3,35,36] focused on a design with a first-wall neutron wall load of $I_w \simeq 20 \text{ MW/m}^2$, and high-coverage, poloidal pumped limiters. This design uses lithium lead, $\text{Pb}_{83}\text{Li}_{17}$, as the coolant and the breeder, ferritic-steel (HT-9) as the structural material, and a thin (0.10 m) steel shield. The magnet system includes closely coupled, copper-alloy TF and poloidal-field (PF) coils. The PF coils include both OH and EF coils. The CRFPR design operates at steady state using OFCD [37,38]. A single-piece FPC maintenance procedure was envisioned. The heaviest components are the PF-coil set at 800 tonne and the reactor torus (first wall, blanket, shield, and TF coils) at 300 tonne.

During the TITAN study, a wide range of FPC configurations were considered and two main engineering design options emerged for detail design: (a) TITAN-I, a self-cooled liquid-lithium design with vanadium alloy (V-3Ti-1Si) as the structural material; and (b) TITAN-II, a “loop-in-pool” configuration with an aqueous solution with dissolved LiNO_3 salt as the coolant and breeder, and ferritic steel alloy 9-C [39] as the structural material. The TITAN-II FPC is submerged in pool of water to achieve a high level of safety assurance. The TITAN-I design incorporates the IBC concept [13], wherein the toroidal magnetic field is produced by poloidal currents conducted in the liquid-lithium coolant, with joule losses being recovered directly in the thermal cycle. The TITAN-II design uses copper-alloy TF and divertor coils. The TITAN designs operate at steady state using OFCD, feature high-recycling toroidal-field divertors for impurity control and particle exhaust [40], and operate at an aggressive first-wall neutron load of 18 MW/m^2 . Because of the small physical size and mass, the TITAN FPCs are made of a few factory-fabricated pieces that are assembled on-site into a single torus, tested to full operational condition, and installed as a single unit in the reactor vault.

In order to eliminate steady-state power consumption in the resistive EF coil (53.5 MW for the CRFPR design [2,3]), the TITAN designs use superconducting (SC) EF coils. This option also allows a more open FPC geometry, which requires higher currents in the EF coils because of the poorer coupling of PF coils to the plasma. The OH and TF coils in TITAN, however, are normal conducting (NC) to retain a compact reactor torus, with the OH-coil set being used and sized for start-up conditions only. Both OH and TF coils (or a subset of their windings) may also serve OFCD functions, depending on the electrical design of the intervening first wall, blanket, and shield.

The systems model described in References [2-3] was expanded for the TITAN study to include a self-consistent treatment of separate OH and EF coils (Figure 3.1-3). The scaling of poloidally symmetric toroidal-field divertors and OFCD was also included in the revised optimization algorithm. The basic computational algorithm remains essentially as described in Reference [3]. As for any model of this nature, the best choices are made on the basis of separate and detailed analyses of various subsystems such as neutronics, plasma equilibrium, OFCD, divertor, and thermal-hydraulic calculations. Some important trade-offs like construction time versus size and complexity, mean-time-to-repair versus mean-time-to-failure as a function of power density and size, and elasticity of nuclear and size economies of scale for key components remain inadequately resolved and in need of future work. Table 3.4-I lists key design variables that were either fixed or varied in the re-optimization of the RFP reactor for the TITAN study.

A typical PSA code output curve is shown on Figure 3.4-1, which displays COE as a function of plasma minor radius, r_p , for fixed aspect ratio, $A = 6.5$, and net power output $P_E = 970$ MWe. The higher dashed curve illustrates the COE based on then-current dollars, and the solid curve illustrates the constant-dollar-mode, which is reported exclusively in the remainder of this section. The minimum-COE design point is denoted by an open circle on the solid curve. It should be noted that the choice of costing mode does not alter the value of plasma radius producing the minimum-COE design point. The minima in the curves result from the trade-off between higher capital cost for larger FPCs as r_p increases and the reduced plant availability factor, p_f , for small values of r_p as neutron first-wall load, I_w , increases for fixed P_E .

A feature of Figure 3.4-1 is the shallowness of the COE versus r_p (and hence, I_w) minimum, although the compressed COE scale should be noted. Nevertheless, increasing I_w from 5 to 10 MW/m² and then to the near-minimum-COE design at $I_w \simeq 18$ MW/m² results only in a 3% and 11% reduction in COE, respectively. Other developmental and operational incentives (*i.e.*, single-piece maintenance) not included in the present costing model may justify the higher- I_w , high-MPD design points that reside closer to the COE minimum.

The variation of the cost of near-minimum-COE design points with plasma aspect ratio, $A = R_T/r_p$, is weak in the range examined ($A = 4$ to 8), as illustrated in Figure 3.4-2. Establishing a maximum grid power of $P_{GRID} \simeq 300$ MWe delivered to the OH coil in the back-bias condition during start-up, and maintaining the peak (inboard) von Mises stress in the OH coil at $\sigma_{OH} \leq 200$ MPa set a limit of $A \geq 5.5$ to 6; a TITAN baseline value of $A = 6.5$ was selected to allow for added start-up flux and provides sufficient symmetrization of the TF for an efficient magnetic-divertor design (Section 4.4).

Table 3.4-I.

**FIXED AND VARIABLE PARAMETERS FOR TITAN REACTOR
OPTIMIZATION AND SENSITIVITY STUDIES**

Parameter	TITAN-I	TITAN-II
Varied Parameters ^(a)		
Plasma aspect ratio	6.5	6.5
Plasma minor radius (m)	0.60	0.60
Poloidal beta	0.20	0.20
Plasma average temperature (keV)	~ 10.	~ 10.
Lawson parameter, $n\tau_E$ (10^{20} s/m ³) ^(b)	1.92	1.92
Reversal parameter, F	-0.10	-0.10
Pinch parameter, Θ ^(c)	1.56	1.56
TF- and divertor-coil options	Cu or IBC	Cu
EF-coil option	SC or NC	SC or NC
EF-coil shield standoff (m)	0.5 (SC), 0.0 (NC)	0.5 (SC), 0.0 (NC)
FPC radiation lifetime, $I_w \tau$ (MWy/m ²)	15.	15.
Plant factor, p_f ^(d)	≤ 0.76	≤ 0.76
Fixed Parameters		
Primary coolant	Liquid lithium	Aqueous solution
Structural material	Vanadium	Ferritic steel (9-C)
Blanket energy multiplication ratio, M_N	0.44	0.35
First-wall, blanket, & shield standoff (m)	0.77	0.50
SC current density, j_c (MA/m ²)	Equation 3.2-37	Equation 3.2-37
Cu current density, j_c (MA/m ²) ^(e)	≤ 50	≤ 50

(a) Nominal design values are given.

(b) Consistent with plasma temperature. Also $n = \sum n_j f_j$ with $f_D = f_T = 0.484$, $f_\alpha = 0.03$, $f_{Xe} = 0.003$; $Z_{eff} = 1.69$.

(c) Consistent with reversal parameter, plasma current, poloidal beta, etc.

(d) Calculated from Equation 3.2-43 and consistent with FPC lifetime, 28 days FPC scheduled maintenance, and 60 d/y of unscheduled maintenance.

(e) Trade-offs between cost of the power supply and cost of copper usually set j_c below this limit. Typically $j_c = 10$ to 15 MA/m².

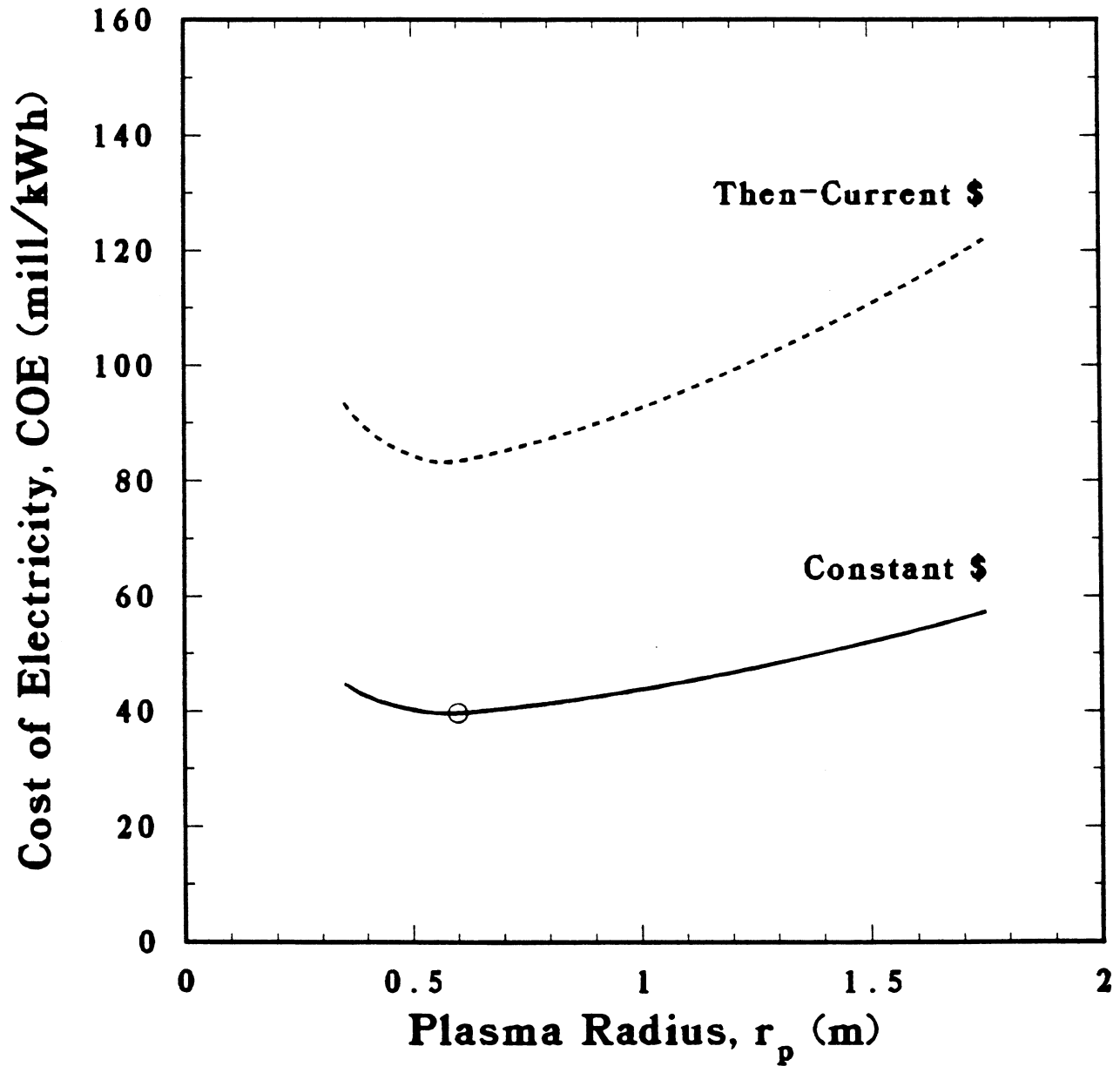


Figure 3.4-1. Dependence of COE on plasma minor radius for constant-dollar and then-current-dollar costing modes analyses. The minimum-COE operating point is denoted by an open circle. The net power output is fixed at $P_E = 970$ MWe and the plasma aspect ratio is $A = 6.5$.

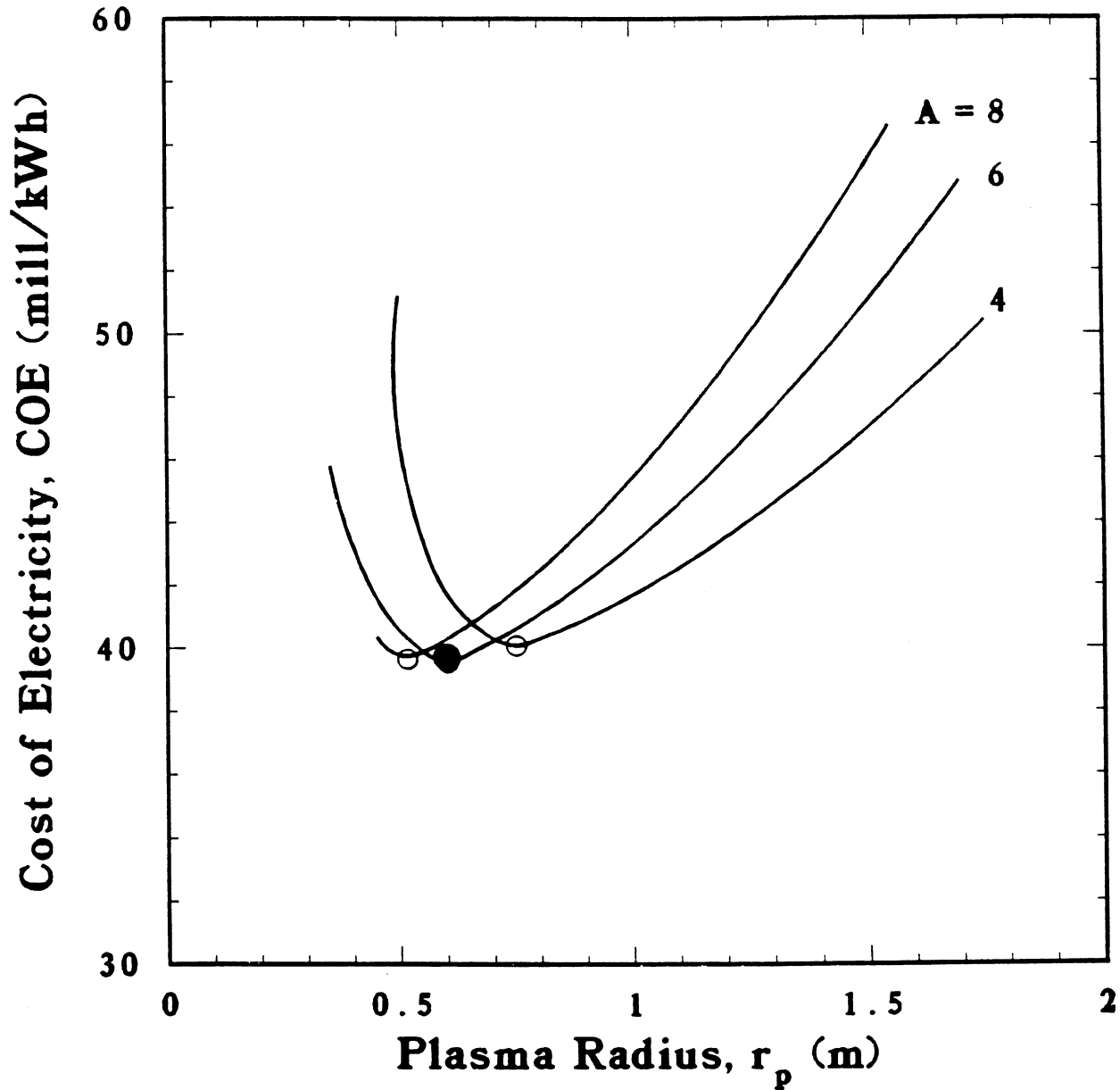


Figure 3.4-2. Dependence of COE on plasma aspect ratio, $A \equiv R_T/r_p$. Minimum-COE design points for each value of A are denoted by open circles. The near-minimum-COE TITAN-I reference design point at $A = 6.5$ and $r_p = 0.60$ m is denoted by a filled circle.

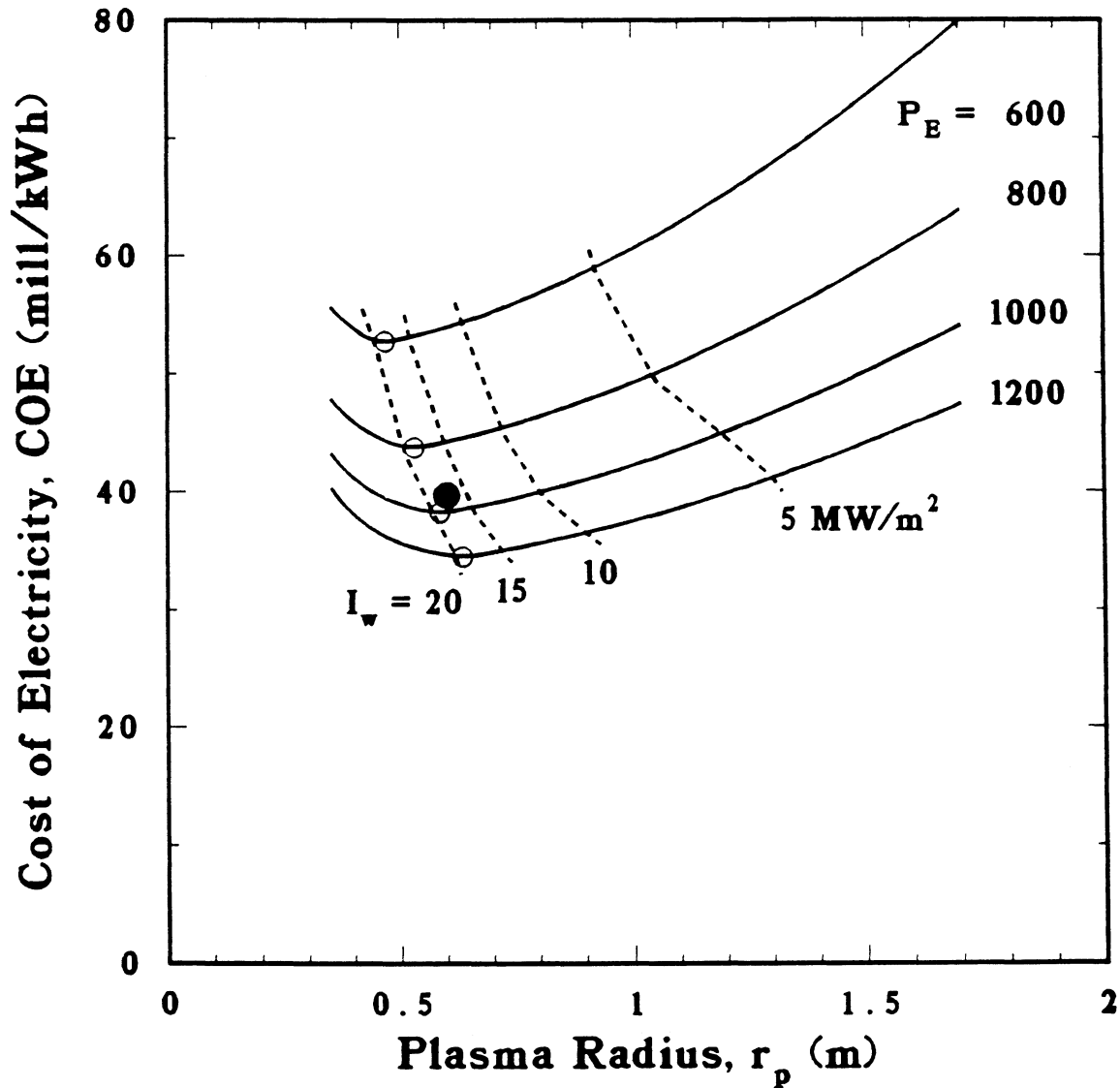


Figure 3.4-3. Dependence of COE on plasma minor radius for a fixed plasma aspect ratio, $A = 6.5$, for various indicated values of net power output, P_E . The crowding of the curves at higher values of P_E is indicative of the nuclear economies of scale built into the cost data base (cf. Table 3.3-III). For each value of P_E , the minimum-COE design point is denoted by an open circle. The dashed lines are contours of constant neutron wall loading, I_w . The near-minimum-COE TITAN-I reference design point at $P_E = 970$ MWe, $I_w = 18.1$ MW/m^2 , and $r_p = 0.60$ m is indicated by the filled circle.

The dependence of COE on P_E given on Figure 3.4-3 is typical of nuclear economies of scale, resulting in smaller marginal cost benefits as P_E increases. The TITAN-I design window is also elaborated in Figure 3.4-3, which displays contours of constant neutron first-wall load, I_w , together with contours of net power output P_E for the indicated fixed parameters. Above values of $I_w \simeq 20 \text{ MW/m}^2$ for the nominal first-wall and blanket fluence lifetime, $I_w\tau = 15 \text{ MWy/m}^2$, faster than annual change-out of the FPC results in plant availability, p_f , reduced below 76% and higher values of COE. Only a modest cost penalty is incurred for operation at lower values of I_w (*i.e.*, down to 10 MW/m^2). Below this value, however, the applicability of a single-piece FPC maintenance approach, which is important to the justification of the nominal value $p_f \simeq 0.76$, becomes questionable. It should be noted that the shallowness of these cost minima is a result of the FPC in TITAN already representing a small percentage of the total direct cost.

The TITAN PSA model was used to characterize several tentative designs before settling on a reference TITAN-I case during an iterative process involving input from the subsystem design activities of the study. Several of these preliminary designs are summarized in Table 3.4-II. Case A is a conventional copper-coil configuration conceptually similar to the CRFPR [2,3]. Case B incorporates the IBC option for both the TF and divertor-field (DF) coils functions, but retains a copper EF-coil pair. Higher recirculating power results in significantly higher neutron first-wall load, I_w , and COE for the same value of net power output, P_E . Case C, the TITAN reference case, retains the IBC option but uses a superconducting EF coil pair to reduce the steady-state recirculating power, offsetting the increased capital cost of the superconducting EF coils to give COE performance nearer that of Case A.

The PSA geometric model (Figure 3.1-3) assumes an annular-shell representation for the OH-coil set. After appropriate magnetics discretization (Section 4.5), a tentative TITAN-I FPC model results. This model is subsequently refined by more detailed engineering analysis (Section 10), and appropriate adjustments are made to a re-calibrated PSA model.

The average neutron wall load for the TITAN-I reference design is $I_w \simeq 18.1 \text{ MW/m}^2$. The NEWLIT code [8] was used to map the poloidal variation of I_w . The volumetric neutron source distribution assumed is illustrated in Figure 3.4-4. The peaking is consistent with the $g_{D\tau} n_i^2(r) \langle \sigma v \rangle_{D\tau} [T_i(r)]$ source distribution of Equation 3.2-1. The outward Shafranov shift of an RFP plasma at the nominal aspect ratio $A = 6.5$ is negligible. For purposes of NEWLIT modeling, the TITAN-I first-wall tube bank is represented by an inscribed polygon with 16 sides. This approximation results in a geometric correction such that $I_w = 18.1 = \Gamma_{av} (16/\pi) \sin(\pi/16)$. The minimum wall load modeled by NEWLIT is

Table 3.4-II.

SUMMARY OF TITAN-I REACTOR DESIGNS^(a,b)

Parameter	Case A	Case B	Ref. Case ^(c)
EF-coil option	Copper	Copper	SC ^(d)
DF-coil option	Copper	IBC ^(e)	IBC ^(e)
TF-coil option	Copper	IBC ^(e)	IBC ^(e)
Plasma Parameters			
Plasma current, I_ϕ (MA)	18.24	18.23	17.82
Plasma ion density, n_i (10^{20} m^{-3})	8.75	9.36	8.93
Plasma electron density, n_e (10^{20} m^{-3})	9.14	9.78	9.33
Poloidal field at plasma surface, $B_\theta(r_p)$ (T)	5.88	6.08	5.94
Thermal diffusivity, χ_E (m^2/s)	0.308	0.330	0.315
Fusion power density, P_F/V_p (MW/m^3)	79.7	91.1	83.0
Plasma ohmic dissipation, P_{OHM} (MW)	28.0	29.8	28.5
Poloidal-Field Quantities			
OH-coil thickness, δ_{OH} (m)	0.23	0.27	0.27
Average minor radius of coil, r_{OH} (m)	1.57	1.57	1.56
OH-coil field, $B_{\theta c}$ (T)	2.24	2.33	2.28
OH-coil current density, j_{OH} (MA/m^2) ^(f)	15.8	13.7	13.1
Mass of OH-coil set, M_{OH} (tonne)	290.	343.	343.
EF-coil current density, j_{EF} (MA/m^2)	6.6	6.1	19.2 ^(d)
Mass of EF-coil set, M_{EF} (tonne)	521.	573.	305.
Poloidal-field stored energy, $W_{M\theta}$ (GJ)	1.8	1.8	5.2
OH-coil dissipation during back-bias (MW)	211.	132.	121.
Toroidal-Field Quantities			
TF-coil thickness, δ_{TF} (m)	0.03	0.28 ^(e)	0.28 ^(e)
Average minor radius of coil, r_{TF} (m)	1.45	0.68	0.68
Mass of TF-coil set, M_{TF} (tonne)	31.	41.	41.
Reversed toroidal field, $-B_{\phi R}$ (T)	0.378	0.391	0.382
Toroidal-field stored energy, $W_{M\phi}$ (GJ)	0.73	0.17	0.16
TF-coil current density, j_{TF} (MA/m^2)	15.8	1.68	1.64
Ohmic dissipation during burn, P_{TF}^Ω (MW)	30.2	28.9	27.6
Mass of DF-coil set, M_{DF} (tonne)	2.0	0.57	0.55
Ohmic dissipation in divertor, P_{DF}^Ω (MW)	12.	145.	142.

Table 3.4-II (Cont'd)

Parameter	Case A	Case B	Ref. Case ^(c)
Engineering Summary			
Neutron first-wall loading, I_w (MW/m ²)	17.4	19.9	18.1
Engineering Q-value, $Q_E = 1/\epsilon$	6.20	3.20	4.02
Fusion power, P_F (MW)	2,207.	2,526.	2,301.
Total thermal power, P_{TH} (MW)	2,630.	3,207.	2,935.
Net electrical power output, P_E (MWe)	970.	970.	970.
Fusion-power-core minor radius, r_s (m)	1.69	1.70	1.70
Masses (tonne)			
· First wall and blanket	41.	41.	41.
· OH-coil "hot shield"	267.	267.	267.
· EF-coil shield	0.	0.	325.
· Total coil set	843.	917.	648.
· Total fusion power core ^(g)	1,152.	1,225.	1,282.
FPC power density, P_{TH}/V_{FPC} (MWt/m ³)	12.0	14.4	13.2
Mass power density, MPD (kWe/tonne) ^(g)	842.	792.	757.
Cost Summary			
Cost of electricity, COE (mill/kWh) ^(h)	37.6	42.3	39.7
Unit direct cost, UDC (\$/kWe)	1,449.	1,627.	1,531.
Total cost, TC (M\$)	2,267.	2,545.	2,396.
FPC unit cost (\$/kg)	147.	144.	146.
Fractions of total direct cost (TDC):			
· Reactor plant equipment, RPE/TDC	0.42	0.45	0.43
· Fusion-power-core cost, FPC/TDC ^(g)	0.12	0.11	0.13

(a) All designs are for baseline parameters given in Table 3.4-I:

$$A = 6.5, R_T = 3.9 \text{ m}, r_p = 0.60 \text{ m}, V_p = 27.7 \text{ m}^3, r_w = 0.66 \text{ m}.$$

(b) $M_N = 1.20$, $\eta_{TH} = 0.44$, and water detritiation system cost $\simeq 5$ M\$.

(c) Iterated basis for detailed elaboration and analysis.

(d) Superconducting coils.

(e) Integrated blanket coil (IBC).

(f) Symmetric bipolar swing ($f_G \equiv I_{OH}^+/I_{OH}^- = 1$),

I_{OH}^+ subsequently decays to zero upon initiation of OFCD.

(g) Includes first wall, blanket, shield, and coils, but not FPC support structures.

(h) Costs reported in constant 1986-dollars, assuming 6 years construction time.

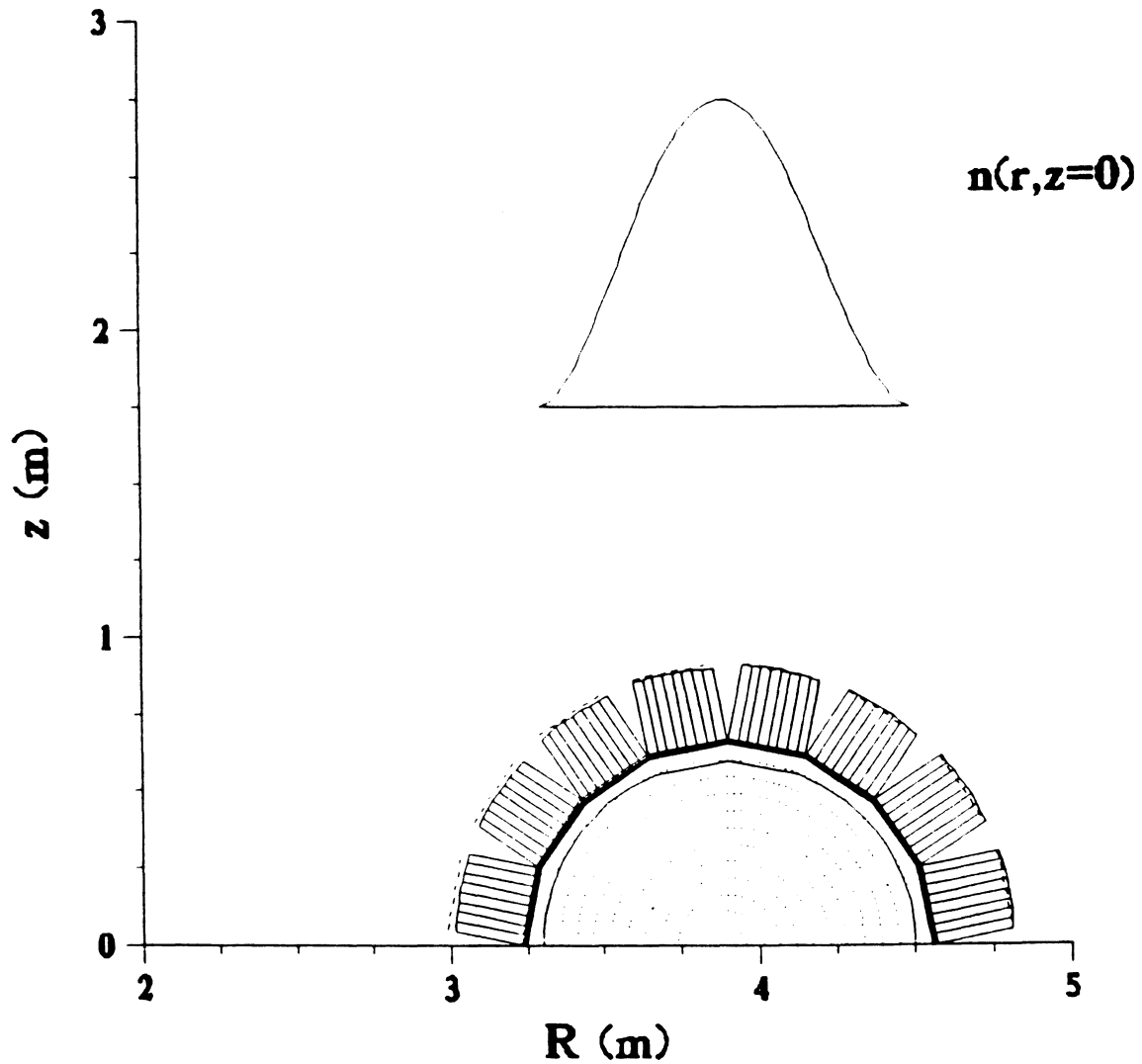


Figure 3.4-4. Un-collided fusion neutron source distribution used in the modeling of the poloidal variation of the neutron wall loading for the TITAN-I reference design point (with $r_p = 0.60$ m, $r_w = 0.66$ m, and $R_T = 3.9$ m) using the NEWLIT code [8]. The first wall is represented by an inscribed polygon with 16 sides.

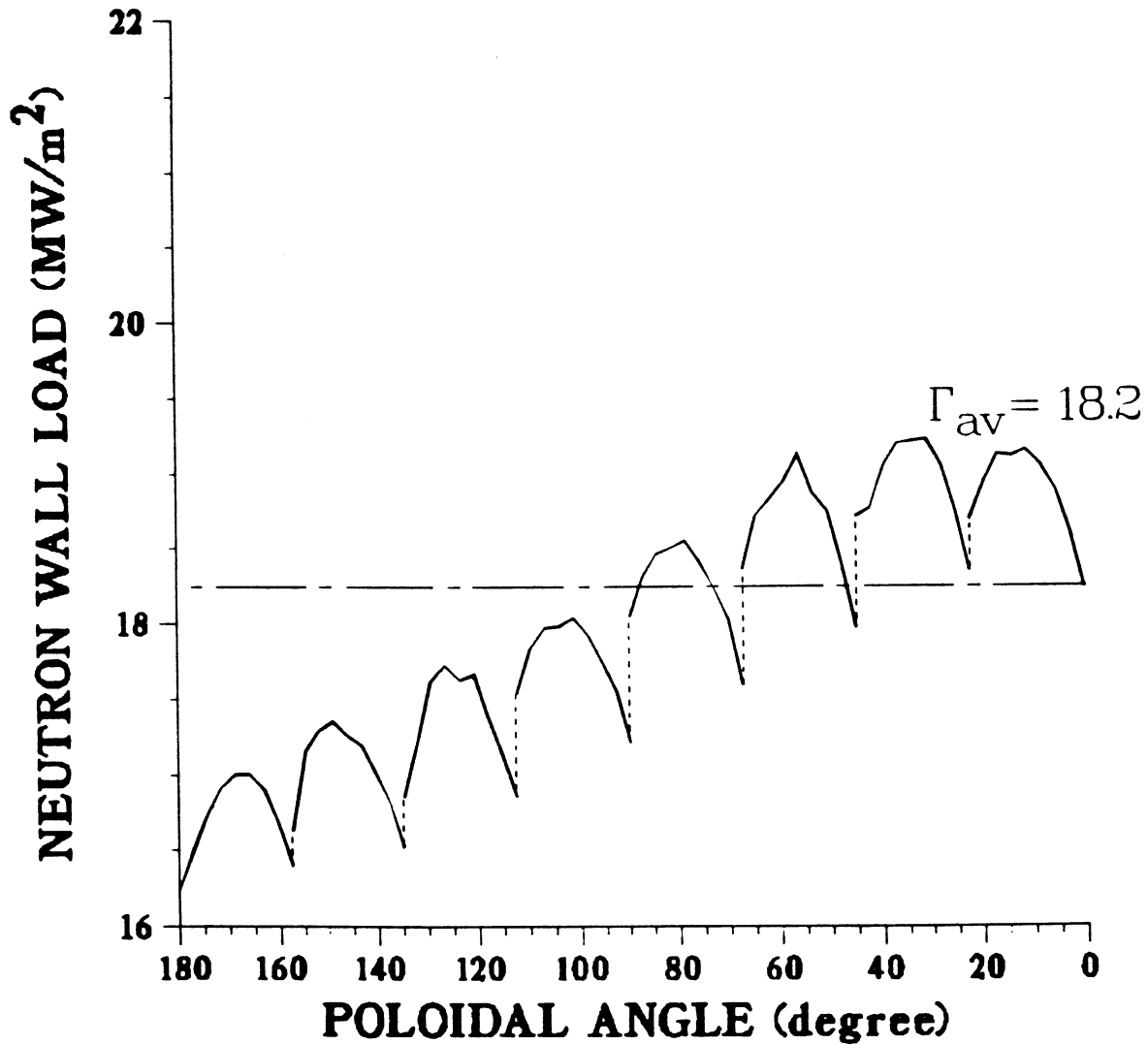


Figure 3.4-5. Poloidal variation of the neutron wall load, I_w , for the TITAN-I reference design point. The inboard and outboard first-wall locations in the equatorial plane occur, respectively, at the poloidal angles $\theta = 180$ and 0 degrees. The fusion power is $P_F = 2300$ MW. The first wall is represented in the NEWLIT code [8] by an inscribed polygon with 16 sides.

16.24 MW/m² on the inboard side at the first wall in the equatorial plane, and the maximum wall load is 19.22 MW/m² at the outboard equatorial plane. The fine structure in the profile shown in Figure 3.4-5 is an artifact of the NEWLIT polygonal approximation and of negligible importance. The general poloidal variation in I_w is sufficiently small for $A = 6.5$. The surface heat-flux distribution resulting from the distributed radiated power, $P_R(\theta) = f_{RAD}(P_\alpha + P_{OHM})$, is qualitatively similar to $P_n(\theta) \propto I_w(\theta)$. Therefore, local peaking of the surface heat load on the first-wall coolant tubes is also small. Peaking in a low-aspect-ratio device is potentially more severe, resulting in a constraint on accessible values of I_w .

3.4.2. Trade-off and Sensitivity Studies

In addition to the TITAN design points emerging from the PSA code, trade-off and sensitivity studies were performed to establish and characterize the “design window” of attractive RFP reactor operation. Several of the key fixed parameters are re-examined with a view toward establishing the sensitivity of the reference design to changes in these parameters.

The reference TITAN-I plasma operating temperature is $T \simeq 10$ keV. Table 3.4-III summarizes the sensitivities of key reactor parameters such as COE, engineering Q-value $Q_E = 1/\epsilon$, and first-wall neutron load I_w on T in the range 10 to 20 keV. The variation of these global parameters is fairly small on this temperature range although a slight peaking nearer to $T \simeq 15$ keV may be indicated, consistent with the peaking of $\langle \sigma v \rangle_{DT}/T^2$ at $T \simeq 13.5$ keV. Separate studies suggest operation at the higher temperatures to maximize the efficiency of OFCD (Section 7). An overriding consideration suggesting the lower values of T , however, was the establishment of a high- f_{RAD} core plasma with edge-plasma conditions consistent with efficient magnetic-divertor operation (Section 5). For fixed values of β_θ and magnetic field, temperature trades off directly with density for constant pressure, but the plasma fusion-power density and neutron wall load, I_w , are nearly constant.

Consistent with the best operation of present-day RFP experiments, the nominal TITAN poloidal-beta value is $\beta_\theta = 0.20$; this value includes only thermalized fusion-product alpha-particle and Xe impurities at $T_{Xe} = 10$ keV. The energetic alpha-particles add about 0.02 to this beta value. The response of the TITAN-I design to lower values of β_θ is shown in Figure 3.4-6. The COE increases as β_θ is decreased which is caused primarily by the need to establish and drive more plasma current, as reflected in increased

OFCD power consumption, increased coil mass, and reduced MPD. Values of β_θ much below ~ 0.1 would result in large increase in COE.

Using the experimental scaling of the confinement time, $\tau_{Ee} \propto I_\phi^\nu r_p^2 f(\beta_\theta)$, the impact of the plasma current scaling exponent, ν , on achieving the minimum-COE TITAN-I design is illustrated in Figure 3.4-7. For each respective constant ν curve, the condition $\tau_E(\text{ECON}) \leq \tau_E(\text{PHYS}) \equiv 2(1/\tau_{Ee} + 1/\tau_{Ei})^{-1}$ with $\tau_{Ei} \simeq 4\tau_{Ee}$ is met to the right (*i.e.*, higher r_p). The accessibility to minimum-COE designs depends on the value of ν . In addition, for ν values much below ~ 0.8 , the demands on the OH-coil system during the ohmic-heating transient to ignition and burn can be serious. Also, it should be noted that the flexibility of operation of the TITAN-I device at lower than nominal power (as for load following or checkout) requires better intrinsic plasma confinement (*i.e.*, higher ν).

Table 3.4-III.

DEPENDENCE OF KEY TITAN-I PARAMETERS ON ION TEMPERATURE^(a)

Ion temperature, T_i (keV)	10 ^(b)	15	20
Lawson parameter, $n\tau_E$ (10^{20} s/m ³)	1.92	1.30	1.10
Electron temperature, T_e (keV)	9.5	14.	19.
Plasma current, I_ϕ (MA)	17.82	17.87	18.60
Fusion power density, P_F/V_p (MW/m ³)	83.0	82.3	82.6
Plasma ion density, n_i (10^{20} m ⁻³)	8.93	5.99	4.87
Neutron wall load, I_w (MW/m ²)	18.11	17.96	18.01
Engineering Q-value, $Q_E = 1/\epsilon$	4.02	4.16	4.11
Cost of electricity, COE (mill/kWh)	39.7	39.5	39.8

(a) Fixed geometric parameters: $A \equiv R_T/r_p = 6.5$ and $r_p = 0.60$ m.

(b) Reference TITAN-I case.

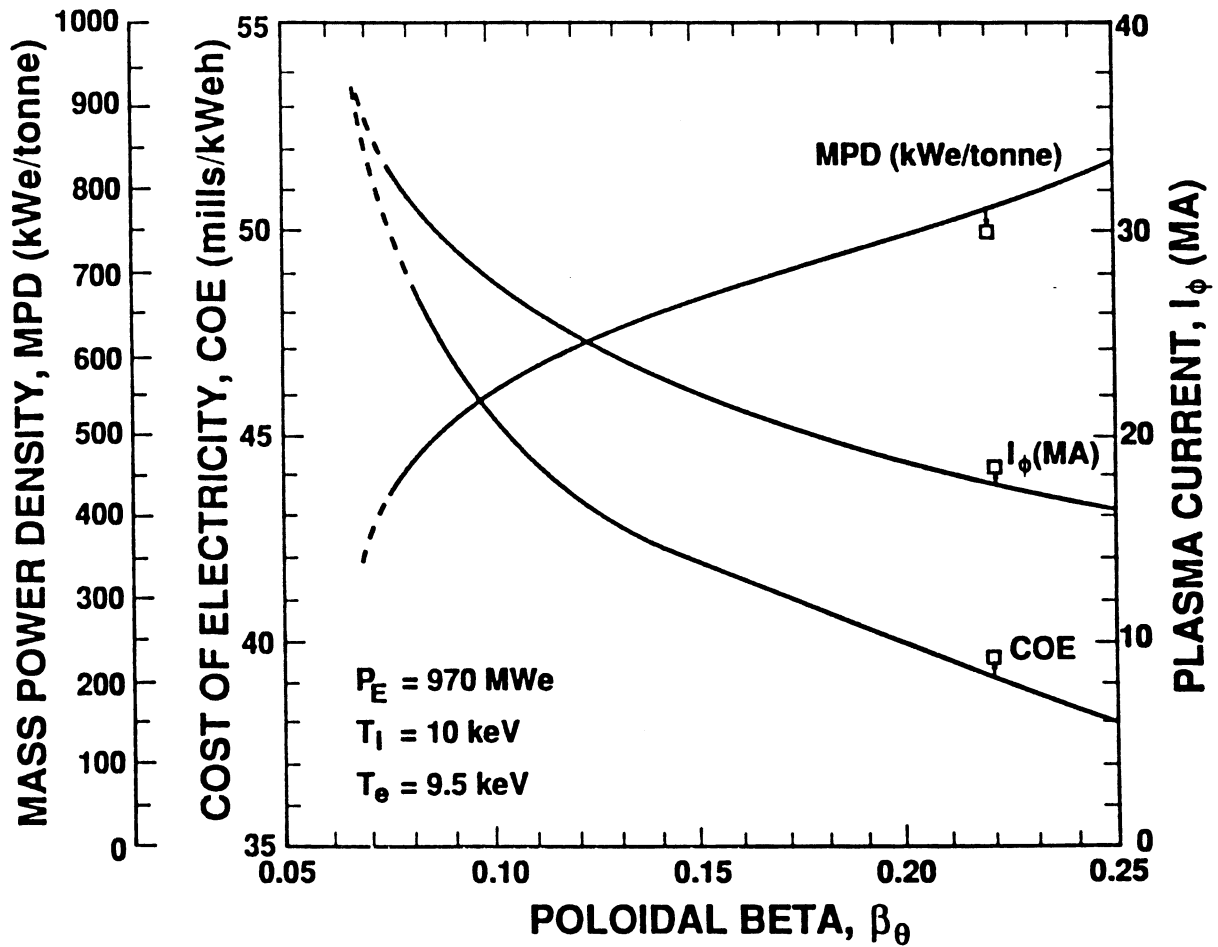


Figure 3.4-6. Dependence of minimum-COE TITAN-I design values on poloidal beta; the near-minimum-COE TITAN-I reference design values are also shown.

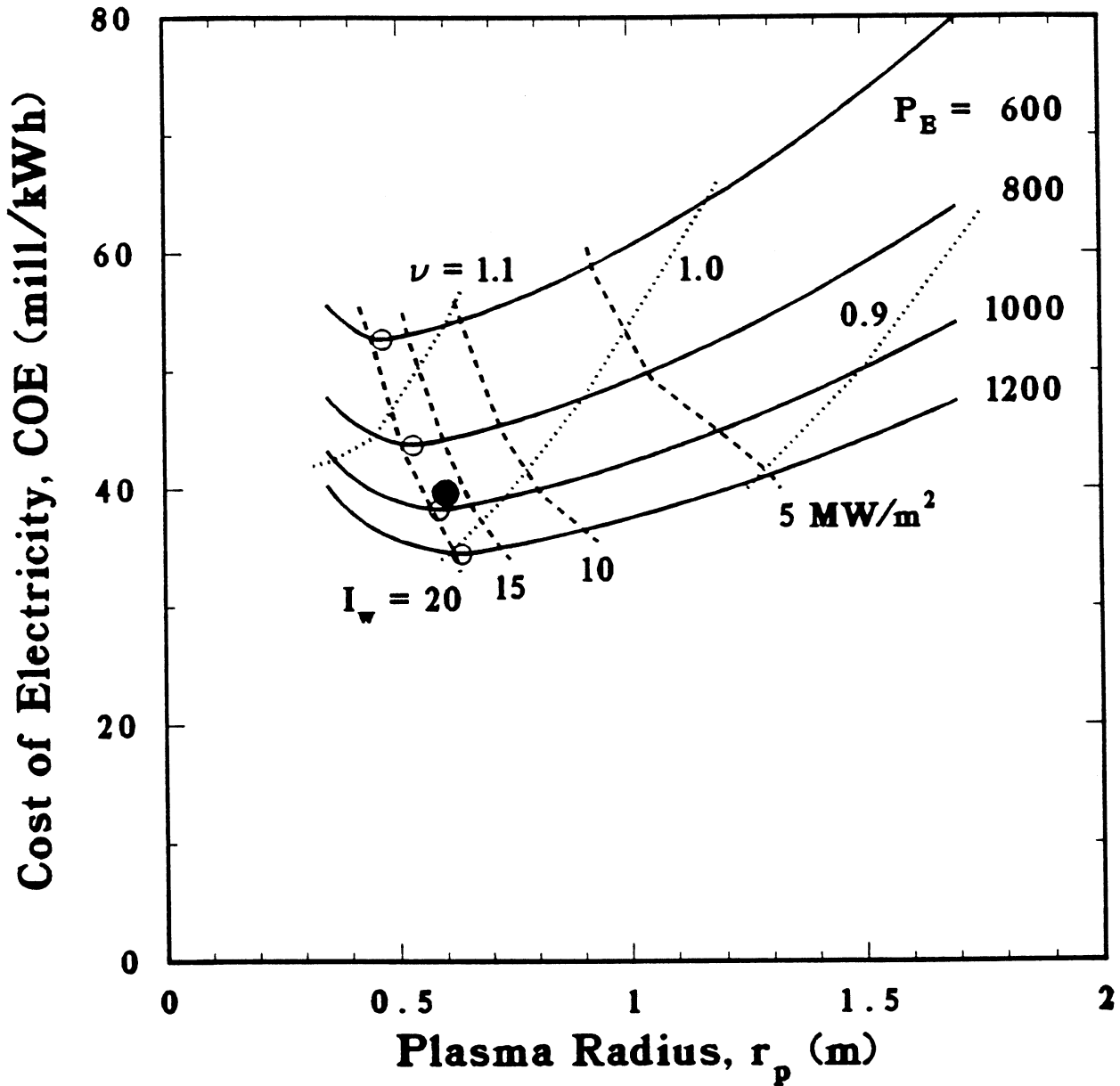


Figure 3.4-7. Parametric trade-off of TITAN-I cost with level of confinement required ($\tau_{Ee} = C_\nu I_\phi^\nu r_p^2 f(\beta_\theta)$, $\tau_{Ei} = 4\tau_{Ee}$), expressed as the magnitude of exponent ν required for $\tau_E(\text{ECON}) \leq \tau_E(\text{PHYS}) = 2(1/\tau_{Ei} + 1/\tau_{Ee})^{-1}$. Accessible design points are to the right of curves of constant ν . Minimum-COE design points with $\tau_E(\text{OPT}) = \tau_E(\text{ECON})$ for fixed net power output P_E are indicated by open circles. The near-minimum-COE TITAN-I reference design at $P_E = 970$ MWe and $I_w = 18.1$ MW/m² is denoted by a filled circle.

The magnitude of the reversal parameter, $F \equiv \bar{B}_\phi(r_p)/\langle B_\phi \rangle$, drives the magnitude of the toroidal field at the coil, and the power required by the magnetic divertor system, P_{DF} , to locally cancel that field. The dependence of key TITAN-I parameters on F is illustrated in Figure 3.4-8. For deeper reversals compared with the reference value $F = -0.1$, the divertor power, P_{DF} , grows linearly and reduces $Q_E = 1/\epsilon$. To maintain the nominal net power output of $P_E = 970$ MWe, the plasma current rises slowly and $I_w \propto I_\phi^4$ increases until $I_w \simeq 20$ MW/m², whereupon the plant availability, p_f , begins to decrease below 0.76 (*cf.* Figure 3.2-2). Because the dissipated power in the divertor and toroidal-field IBC sets is recovered in the thermal cycle, this power can actually displace some primary fusion power, resulting in somewhat lower values of I_w near $F = -0.3$. The current-drive efficiency, I_ϕ/P_{CD} , also decreases as F becomes more negative, further lowering Q_E , although it should be mentioned that a self-consistent modeling of the OFCD system was not done at these deeper values of F . The nominal value of F in this study was not raised above -0.10 so as to provide a reasonable margin for the OFCD oscillations in F without loss of reversal altogether. Further, more exact (coupled) work in this area is warranted.

Figures 3.4-9 and 3.4-10 show the impact on COE of parametrically increasing the resulting poloidal-flux consumption as the ramp-up rise time, τ_R , is increased, with the main cost drivers being the OH-coil power supply (power-grid-driven rectifiers at 25\$/kVA) and the increased coil mass; the increased power, current, and von Mises stress in the OH coil, σ_{OH} , are also shown for both symmetric ($f_G = 1$) and asymmetric ($f_G = 0.2$) current swings. To provide for the increased poloidal-flux consumption as τ_R is increased, a deeper back-bias current must be provided (*i.e.*, higher I_{OH}^-). For the symmetric case, $I_{OH} \equiv I_{OH}^- = I_{OH}^+$. The resistive flux consumption in the plasma during start-up scales as $f_{RES} L_p I_\phi$ and is directly proportional to τ_R as given by Equation 3.2-39.

The dependence of OH-coil back-bias stress, σ_{OH} , and OH-coil power-supply requirement is illustrated in Figure 3.4-11. For the superconducting EF-coil option selected for TITAN, a symmetric OH-coil current swing ($f_G = 1$) is preferred from the viewpoint of minimizing σ_{OH} and P_{OH} (*cf.* Equation 3.2-40). The cost of the copper OH-coil power supply (25\$/kVA) does not result in a significant cost impact for the values of f_G examined. A model that included a thicker value of δ_{OH} (as f_G decreases to prevent σ_{OH} from increasing) would provide additional cost incentive for the choice of $f_G \simeq 1$ for TITAN. A copper EF-coil option (*cf.* CRFPR) leads to a preference for $f_G \simeq 0.2$.

The dependence of TITAN-I operating parameters on the assumed efficiency of the OFCD power supply, monitored by a circuit Q-value, Q_{PS} , is illustrated in Figure 3.4-12. For a range of values $Q_{PS} > 75$, performance is relatively insensitive to Q_{PS} . Below

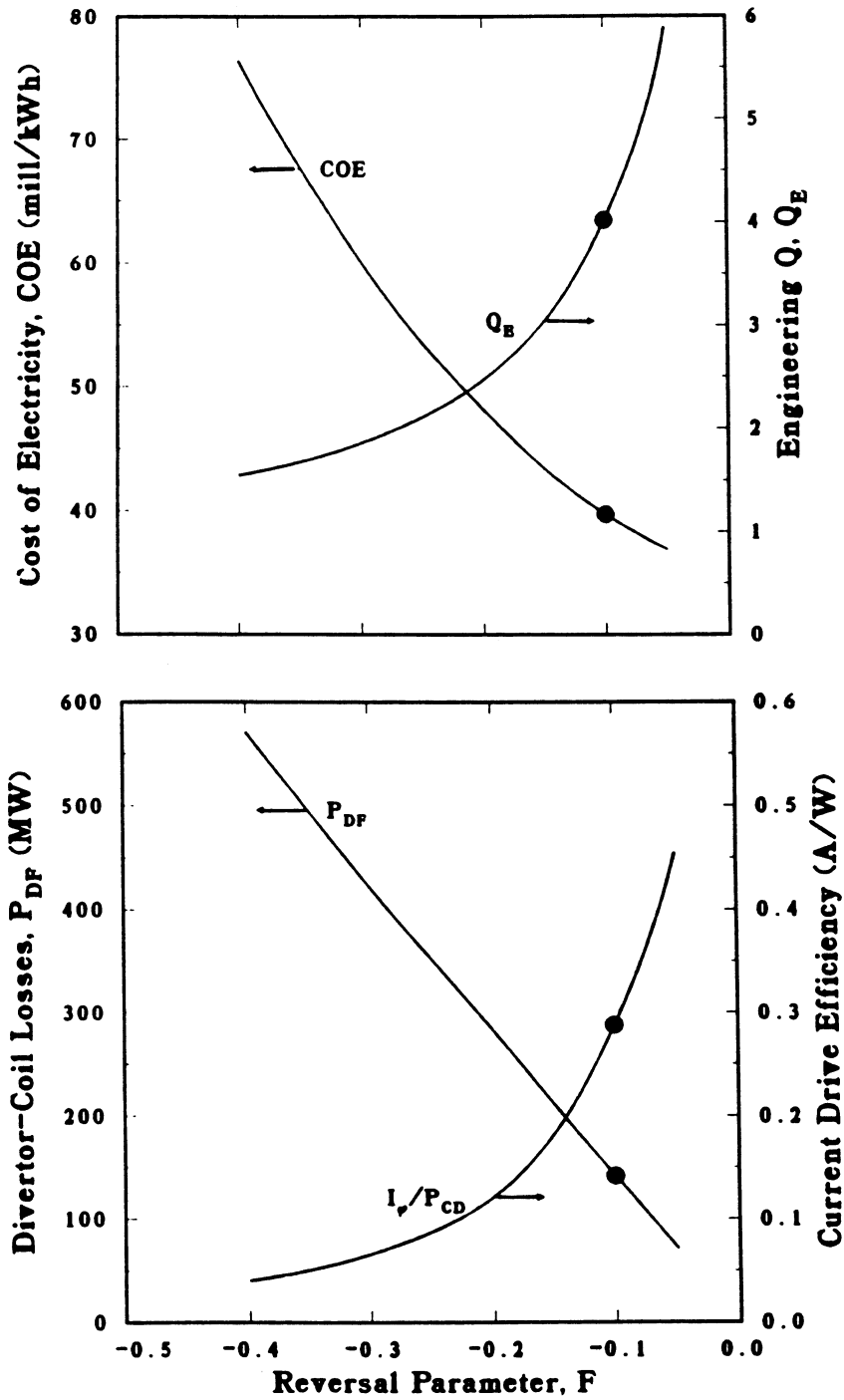


Figure 3.4-8. Impact of the reversal parameter on the overall TITAN-I design and cost. The TITAN-I reference design at $F = -0.1$ is denoted by a filled circle.

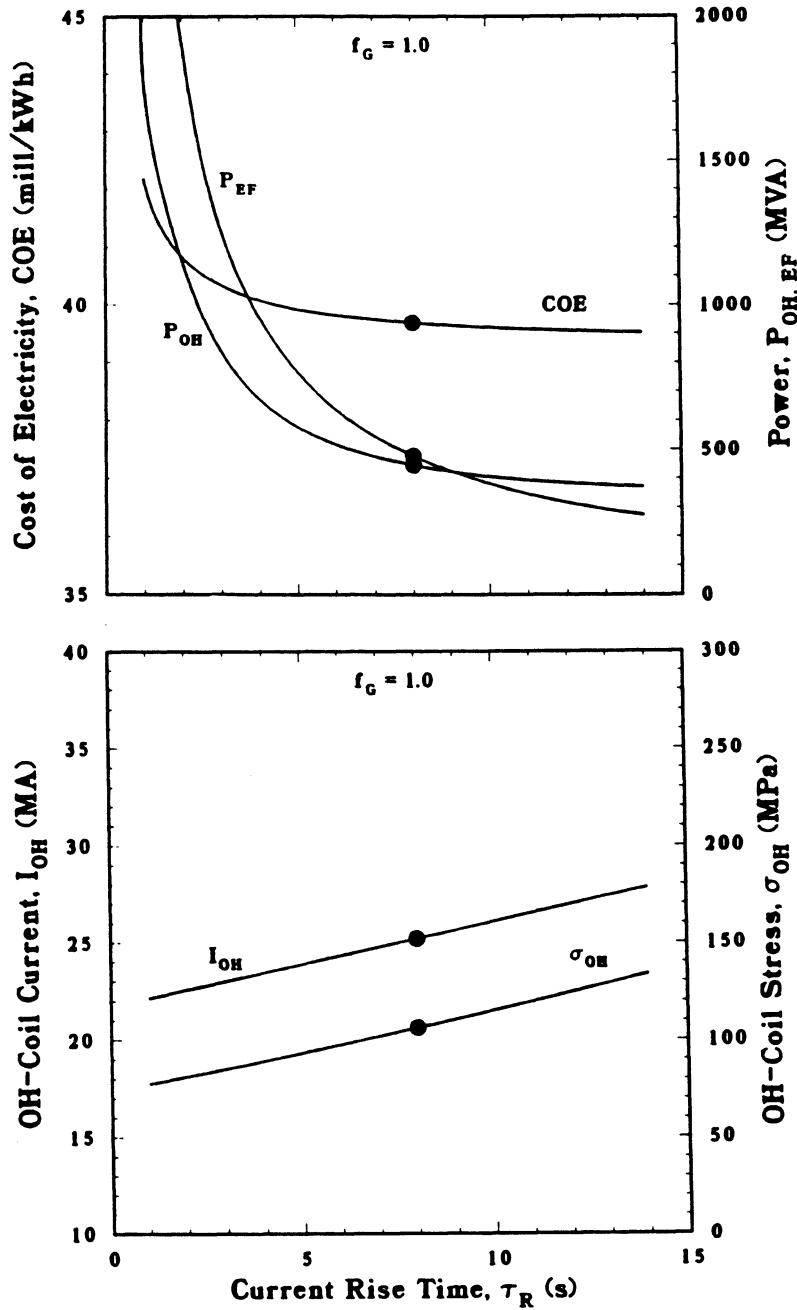


Figure 3.4-9. Dependence of COE and main design parameters (PF-coil power, OH-coil current and stress) on resistive poloidal flux consumption for the TITAN-I design expressed in terms of nominal current rise time for a symmetric back-biased flux swing ($f_G = 1.0$). The TITAN-I reference design is denoted by a filled circle at $\tau_R = 8$ s.

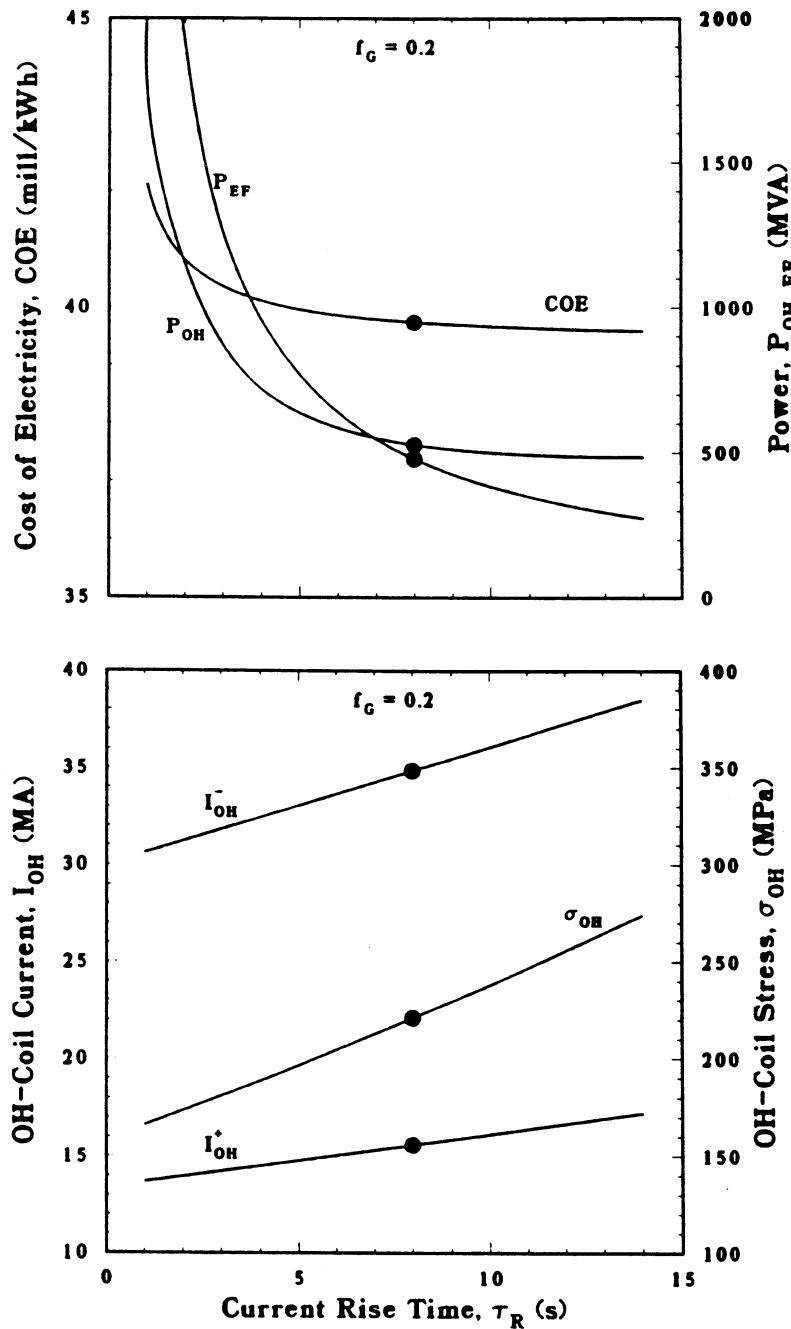


Figure 3.4-10. Dependence of COE and main design parameters (PF-coil power, OH-coil current and stress) on resistive poloidal flux consumption for the TITAN-I design expressed in terms of nominal current rise time for an asymmetric back-biased flux swing ($f_G = 0.2$). The TITAN-I reference design is denoted by a filled circle at $\tau_R = 8$ s.

$Q_{PS} \simeq 50$, however, the OFCD system becomes inefficient and the recirculating power fraction, $\epsilon = 1/Q_E$, begins to increase significantly. As a result, higher values of neutron wall load, I_w , is needed to maintain $P_E = 970$ MWe and higher values of COE as p_f drops below 0.76 (cf. Figure 3.2-5).

Generally, the TITAN-I design point is fairly robust and insensitive to perturbation in values of key parameters, whether physics or engineering. Most such choices are fairly conservative and are grounded in experimental performance (Section 3.3) or engineering practice. Incorporation of the IBC option for the TITAN-I divertor coils introduces a significant recirculating power contribution, which is offset by the negligible joule losses of the superconducting EF-coil set, in contrast to the all-copper-coil CRFPR. The impact of using expensive (250 \$/kg) V-alloy structures in the TITAN-I FPC for safety and environmental reasons is mitigated by the small physical size and impact of the FPC on total cost.

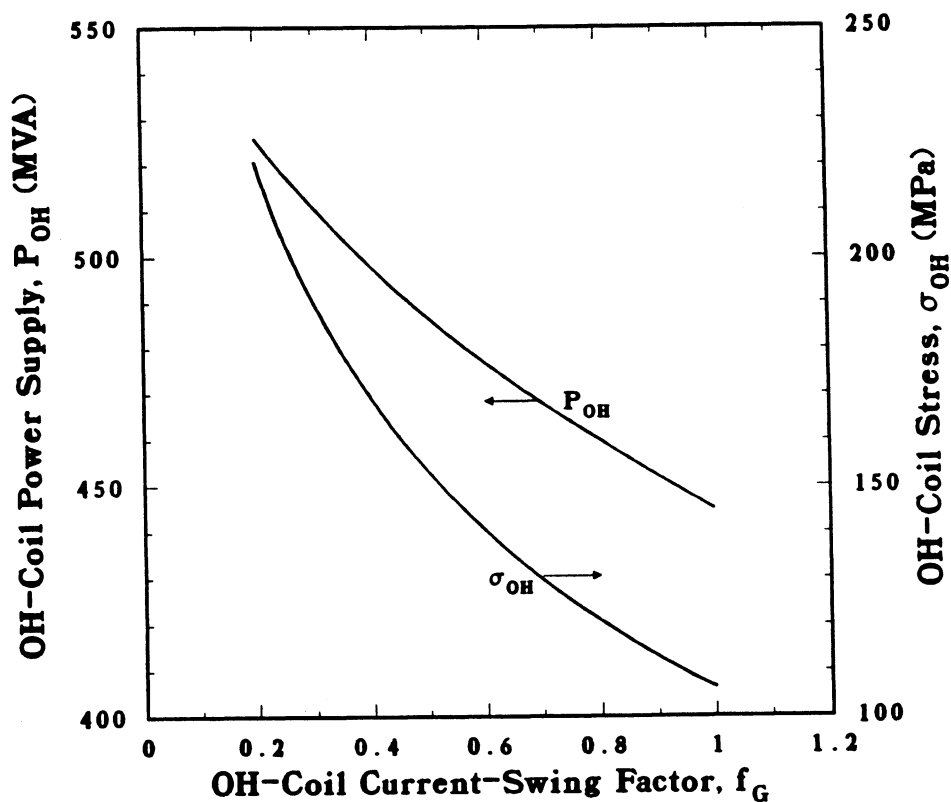


Figure 3.4-11. Dependence of OH-coil back-bias stress and OH-coil power-supply requirement on the OH-coil current-swing symmetry factor, $f_G \equiv I_{OH}^+ / I_{OH}^-$, for TITAN-I.

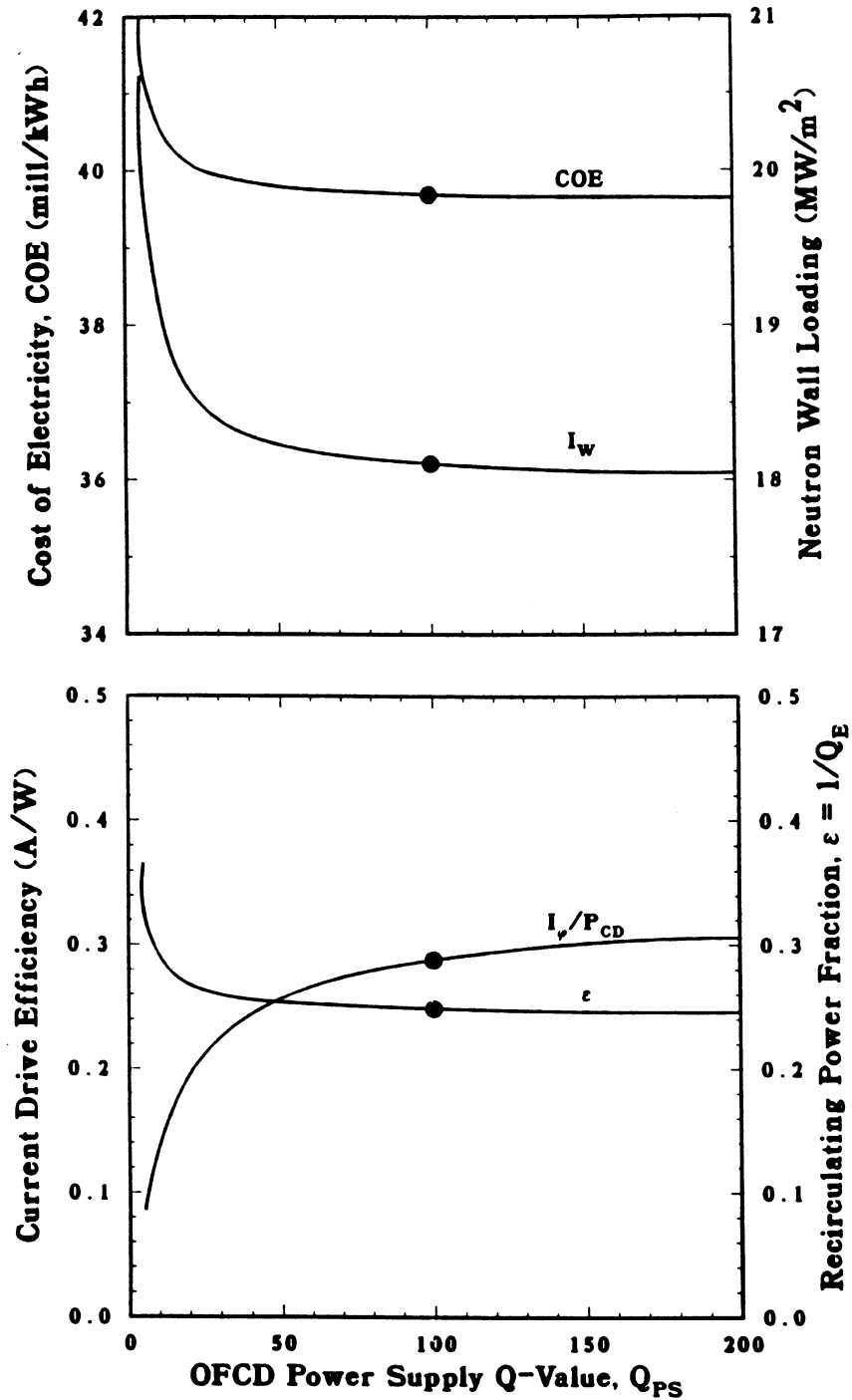


Figure 3.4-12. Impact of OFCD power supply Q-value on TITAN-I operating parameters. The TITAN-I reference case is denoted by a filled circle at $Q_{PS} = 100$.

3.5. TITAN-II DESIGN POINT

3.5.1. Design-Point Selection

The TITAN-II FPC design is an aqueous loop-in-pool concept with a dissolved Li salt (LiNO_3) as the breeder, a Be neutron multiplier, and a reduced activation, high-strength ferritic steel 9-C [39] as the structural material. The complete FPC and the primary coolant system are submerged in a pool of low-temperature, low-pressure water to achieve passive safety. The TITAN-II pool configuration, therefore, provides an alternative approach to inherently safe operation of an RFP reactor, but does not require a significantly different plasma performance or FPC configuration. The TITAN-I IBC configuration is replaced by a more conventional blanket, hot-shield, TF-coil configuration in TITAN-II.

The full coil optimization procedure of the PSA code (Section 3.1) applies to the TITAN-II FPC configuration. The overall coil thickness, δ_c , including the copper TF-coil thickness, δ_{TF} , followed by a gap thickness, $g_{TF/OH}$, and the homogenized OH-coil-set thickness, δ_{OH} . The overall coil thickness is varied to obtain a minimum-COE design point, trading the cost of the recirculating power (joule dissipation) in the TF-coil set with the direct cost of the FPC. The dissipated power in the TF-coil set, P_{TF}^Ω , decreases monotonically as the TF-coil thickness, δ_{TF} , is allowed to increase and the current density, j_{TF} , decreases for relatively fixed values of I_{TF} and $B_\phi = \mu_o I_{TF}/(2\pi R_T)$.

The TITAN-II plasma aspect ratio, A , is retained at 6.5 to facilitate comparison with TITAN-I. As a function of minor plasma radius, r_p , the minimum-COE design point occurs at $r_p = 0.575 \text{ m}$ and corresponding neutron wall load, $I_w = 19.58 \text{ MW/m}^2$, for a fixed net power output, $P_E = 900 \text{ MWe}$. It was decided to move slightly off of the minimum-COE design point to $r_p = 0.60 \text{ m}$ (the same value as used for TITAN-I, which is itself slightly off of its own minimum-COE design point) in order to obtain nearly equal values of $I_w \simeq 18 \text{ MW/m}^2$ and corresponding surface heat fluxes for both TITAN-I and TITAN-II. It is not possible to simultaneously achieve equal values of net power output, P_E (970 MWe for TITAN-I and 900 MWe for TITAN-II), while fixing the FPC geometry because of the differences in power flows between the two TITAN reactor embodiments. The dependence of COE on coil thickness is illustrated on Figure 3.5-1 for both the minimum-COE ($r_p = 0.575 \text{ m}$) and near-minimum-COE TITAN-II reference case ($r_p = 0.60 \text{ m}$). The PSA code searches to find the total coil thickness, δ_c , and partition, δ_{TF}/δ_{OH} , that minimizes the overall COE. For each value of r_p , there exists a similar, but shifted, curve of COE versus δ_c . The greatly expanded COE scale of Figure 3.5-1 exaggerates the sharpness of the minima of these curves.

Table 3.5-I.
SUMMARY OF TITAN-II REACTOR DESIGNS^(a,b)

Parameter	With IHX ^(c)	Without IHX ^(c)
EF-coil option	SC ^(d)	SC ^(d)
DF-coil option	Copper	Copper
TF-coil option	Copper	Copper
Plasma Parameters		
Plasma current, I_ϕ (MA)	17.80	17.80
Plasma ion density, n_i (10^{20} m^{-3})	8.91	8.91
Plasma electron density, n_e (10^{20} m^{-3})	9.31	9.31
Poloidal field at plasma surface, $B_\theta(r_p)$ (T)	5.93	5.93
Thermal diffusivity, χ_E (m^2/s)	0.314	0.314
Fusion power density, P_F/V_p (MW/ m^3)	82.6	82.6
Plasma ohmic dissipation, P_{OHM} (MW)	28.5	28.5
Poloidal-Field Quantities		
OH-coil thickness, δ_{OH} (m)	0.38	0.37
Average minor radius of coil, r_{OH} (m)	1.37	1.37
OH-coil field, $B_{\theta c}$ (T)	2.60	2.61
OH-coil current density, j_{OH} (MA/ m^2) ^(e)	9.1	9.2
Mass of OH-coil set, M_{OH} (tonne)	420.	414.
EF-coil current density, j_{EF} (MA/ m^2)	20.5 ^(d)	20.5 ^(d)
Mass of EF-coil set, M_{EF} (tonne)	247.	247.
Poloidal-field stored energy, $W_{M\theta}$ (GJ)	4.1	4.1
OH-coil dissipation during back-bias (MW)	106.	107.
Toroidal-Field Quantities		
TF-coil thickness, δ_{TF} (m)	0.047	0.046
Average minor radius of coil, r_{TF} (m)	1.11	1.11
Mass of TF-coil set, M_{TF} (tonne)	41.	41.
Reversed toroidal field, $-B_{\phi R}$ (T)	0.381	0.381
Toroidal-field stored energy, $W_{M\phi}$ (GJ)	0.43	0.43
TF-coil current density, j_{TF} (MA/ m^2)	9.1	9.1
Ohmic dissipation during burn, P_{TF}^Ω (MW)	13.4	13.6
Mass of DF-coil set, M_{DF} (tonne)	2.0	2.0
Ohmic dissipation in divertor, P_{DF}^Ω (MW)	12.	12.

Table 3.5-I (Cont'd)

Parameter	With IHX ^(c)	Without IHX ^(c)
Engineering Summary		
Neutron first-wall loading, I_w (MW/m ²)	18.0	18.0
Engineering Q-value, $Q_E = 1/\epsilon$	7.22	7.20
Fusion power, P_F (MW)	2,289.	2,290.
Total thermal power, P_{TH} (MW)	2,985.	2,986.
Net electrical power output, P_E (MWe)	900.	900.
Fusion-power-core minor radius, r_s (m)	1.56	1.55
Masses (tonne)		
· First wall and blanket	21.	21.
· OH-coil "hot shield"	106.	106.
· EF-coil shield	287.	286.
· Total coil set	711.	704.
· Total fusion power core ^(f)	1,125	1,117.
FPC power density, P_{TH}/V_{FPC} (MWt/m ³)	16.0	16.1
Mass power density, MPD (kWe/tonne) ^(f)	800.	806.
Cost Summary		
Cost of electricity, COE (mill/kWh) ^(g)	40.2	38.0
Unit direct cost, UDC (\$/kWe)	1,635.	1,543.
Total cost, TC (M\$)	2,347.	2,488.
FPC unit cost (\$/kg)	118.	119.
Fractions of total direct cost (TDC):		
· Reactor plant equipment, RPE/TDC	0.51	0.48
· Fusion-power-core cost, FPC/TDC ^(f)	0.09	0.10

(a) All designs are for baseline parameters given in Table 3.4-I:

$$A = 6.5, R_T = 3.9 \text{ m}, r_p = 0.60 \text{ m}, V_p = 27.7 \text{ m}^3, r_w = 0.66 \text{ m}.$$

(b) $M_N = 1.36$, $\eta_{TH} = 0.35$, and water detritiation system cost $\simeq 140$ M\$.

(c) Intermediate heat exchanger (IHX) loop.

(d) Superconducting coils.

(e) Symmetric bipolar swing ($f_G \equiv I_{OH}^+/I_{OH}^- = 1$),

I_{OH}^+ subsequently decays to zero upon initiation of OFCD.

(f) Includes first wall, blanket, shield, and coils, but not FPC support structures.

(g) Costs reported in constant 1986-dollars, assuming 6 years construction time.

Two TITAN-II options are summarized on Table 3.5-I, the first including an intermediate heat exchange (IHX) loop and the second without it. Because of the significant cost savings and because of no significant adverse consequences on the area of tritium removal and safety (Section 16, 18, and 19), the second option was selected as the TITAN-II reference design. The deletion of the IHX system increases the relative impact of the FPC on the total capital cost, resulting in a small reduction in the optimal coil thickness and changes in other parameters leading to a slightly different near-minimum-COE configuration.

Plasma parameters for TITAN-II are quite close to those of TITAN-I so some of the plasma engineering effort has not been duplicated. Magnetic-divertor performance (Section 4) and OFCD results (Section 7) are modified somewhat by the influence of a different coil set.

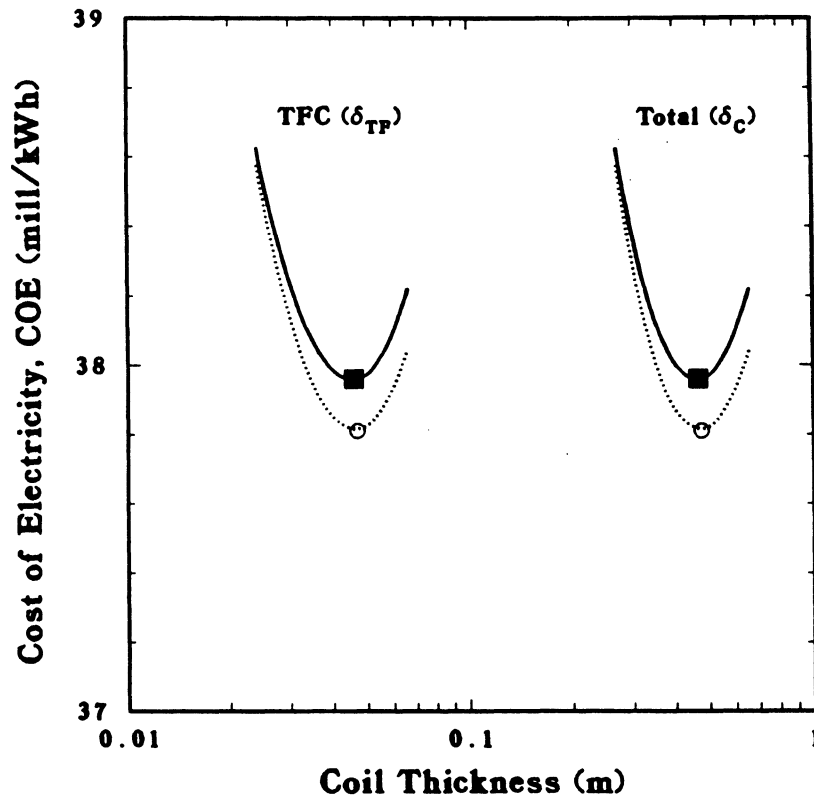


Figure 3.5-1. Dependence of COE on coil thickness at a fixed net power output, $P_E = 900$ MWe. The minimum-COE case ($r_p = 0.575$ m and $I_w = 19.58$ MW/m²) is denoted by an open circle. The TITAN-II near-minimum-COE reference case ($r_p = 0.60$ m and $I_w = 18.0$ MW/m²) is shown as filled square.

3.5.2. Trade-off and Sensitivity Studies

Because the TITAN-I and TITAN-II embodiments share similar plasma configurations, it is not necessary to repeat the temperature, poloidal beta, and reversal parameter variations considered in Section 3.4.2. The rationale of the choice of a superconducting EF-coil set for TITAN-I remains valid for TITAN-II although it is significantly weakened by the reduced lost power in the TITAN-II copper-alloy divertor coil set (~ 12 MW) relative to the divertor IBC selected for TITAN-I which consumes $(1 - \eta_{TH}) \times 145 = 81$ MW.

Several representative TITAN-II design options are summarized in Table 3.5-II. Case A includes a copper EF-coil set similar to the TITAN-I Case A of Table 3.4-II. The large water-detritiation-system cost of TITAN-II (~ 140 M\$) results in a ~ 2 mill/kWh COE penalty, offsetting the cost savings of lower FPC blanket and shield costs (9-C versus V alloy). Case B incorporates a superconducting EF-coil set and an exaggerated gap between TF and OH coil sets, $g_{TF/OH} = 0.31$ m. For this case, the TITAN-II OH-coil set is nearly coincident with that of TITAN-I, substituting a water-filled gap for part of the thicker blanket and shield annulus of TITAN-I. A penalty associated with this option is less-than-ideal coupling of the OH-coil set to the plasma and higher COE relative to the reference case, so this option was de-emphasized. Case C includes a nominal gap, $g_{TF/OH} = 0.05$ m and an asymmetric OH-coil current swing characterized by $f_G \equiv I_{OH}^+/I_{OH}^- = 0.2$. The TITAN-II reference case, with the lowest COE projection of these four options, has a symmetric OH-coil swing ($f_G = 1.0$).

3.6. SUMMARY AND CONCLUSIONS

The operating space of a compact RFP reactor has been examined using a comprehensive parametric systems model which includes the evolving state of knowledge of the physics of RFP confinement and embodies the TITAN-I and TITAN-II engineering approaches. Two key figures of merit, the cost of electricity (COE) and mass power density (MPD), are monitored by the parametric systems model, both of which are displayed in Figure 3.6-1 as functions of the neutron wall loading. Figure 3.6-1 shows that the COE is relatively insensitive to wall loadings in the range of 10 to 20 MW/m² with a shallow minimum at about 19 MW/m². Mass power density is found to increase monotonically with the wall load. For designs with a neutron wall load larger than about 10 MW/m², the FPC is physically small enough such that single-piece FPC maintenance is feasible. These considerations point to a design window for compact RFP reactors with loading in the range of 10 to 20 MW/m². The TITAN-class RFP reactors in this design window

Table 3.5-II.

SUMMARY OF TITAN-II REACTOR DESIGNS^(a,b)

Parameter	Case A ^(c)	Case B ^(d)	Case C ^(c,e)	Ref. Case ^(f)
EF-coil option	Copper	SC ^(g)	SC ^(g)	SC ^(g)
DF-coil option	Copper	Copper	Copper	Copper
TF-coil option	Copper	Copper	Copper	Copper
Plasma Parameters				
Plasma current, I_ϕ (MA)	17.89	17.83	17.82	17.80
Plasma ion density, n_i (10^{20} m^{-3})	9.00	8.94	8.93	8.91
Plasma electron density, n_e (10^{20} m^{-3})	9.40	9.34	9.33	9.31
Poloidal field at plasma surface, $B_\theta(r_p)$ (T)	5.96	5.94	5.94	5.93
Thermal diffusivity, χ_E (m^2/s)	0.317	0.315	0.315	0.314
Fusion power density, P_F/V_p (MW/ m^3)	84.3	83.2	83.0	82.6
Plasma ohmic dissipation, P_{OHM} (MW)	28.7	28.6	28.5	28.5
Poloidal-Field Quantities				
OH-coil thickness, δ_{OH} (m)	0.22	0.31	0.44	0.37
Average minor radius of coil, r_{OH} (m)	1.27	1.59	1.39	1.37
OH-coil field, $B_{\theta c}$ (T)	2.82	2.25	2.56	2.61
OH-coil current density, j_{OH} (MA/ m^2)	16.1 ^(f)	11.4 ^(f)	10.8 ^(e)	9.2 ^(f)
Mass of OH-coil set, M_{OH} (tonne)	226.	403.	500.	414.
EF-coil current density, j_{EF} (MA/ m^2)	4.6	20.2 ^(g)	20.4 ^(g)	20.6 ^(g)
Mass of EF-coil set, M_{EF} (tonne)	674.	259.	251.	247.
Poloidal-field stored energy, $W_{M\theta}$ (GJ)	1.4	4.4	4.2	4.1
OH-coil dissipation during back-bias (MW)	181.	153.	176.	107.
Toroidal-Field Quantities				
TF-coil thickness, δ_{TF} (m)	0.026	0.037	0.039	0.046
Average minor radius of coil, r_{TF} (m)	1.10	1.10	1.10	1.11
Mass of TF-coil set, M_{TF} (tonne)	23.	33.	35.	41.
Reversed-toroidal field, $-B_{\phi R}$ (T)	0.383	0.382	0.382	0.381
Toroidal-field stored energy, $W_{M\phi}$ (GJ)	0.43	0.43	0.43	0.43
TF-coil current density, j_{TF} (MA/ m^2)	16.1	11.4	10.8	9.2
Ohmic dissipation during burn, P_{TF}^Ω (MW)	23.6	16.8	15.9	13.6
Mass of DF-coil set, M_{DF} (tonne)	2.0	2.0	2.0	2.0
Ohmic dissipation in divertor, P_{DF}^Ω (MW)	12.	12.	12.	12.

Table 3.5-II (Cont'd)

Parameter	Case A ^(c)	Case B ^(d)	Case C ^(c,e)	Ref. Case ^(f)
Engineering Summary				
Neutron first-wall loading, I_w (MW/m ²)	18.4	18.1	18.1	18.0
Engineering Q-value, $Q_E = 1/\epsilon$	6.41	6.92	7.00	7.20
Fusion power, P_F (MW)	2,336.	2,305.	2,300.	2,290.
Total thermal power, P_{TH} (MW)	3,047.	3,006.	3,000.	2,986.
Net electrical power output, P_E (MWe)	900.	900.	900.	900.
Fusion-power-core minor radius, r_s (m)	1.38	1.74	1.70	1.55
Masses (tonne)				
· First wall and blanket	21.	21.	21.	21.
· OH-coil "hot shield"	91.	91.	106.	106.
· EF-coil shield	0.	295.	289.	286.
· Total coil set	926.	697.	787.	704.
· Total fusion power core ^(h)	1,053.	1,119.	1,204.	1,117.
FPC power density, P_{TH}/V_{FPC} (MWt/m ³)	20.8	12.9	15.0	16.1
Mass power density, MPD (kWe/tonne) ^(h)	854.	804.	747.	806.
Cost Summary				
Cost of electricity, COE (mill/kWh) ⁽ⁱ⁾	39.8	38.4	38.5	38.0
Unit direct cost, UDC (\$/kWe)	1,617.	1,561.	1,563.	1,543.
Total cost, TC (M\$)	2,608.	2,267.	2,269.	2,239.
FPC unit cost (\$/kg)	118.	119.	116.	119.
Fractions of total direct cost (TDC):				
· Reactor plant equipment, RPE/TDC	0.50	0.48	0.49	0.48
· Fusion-power-core cost, FPC/TDC ^(h)	0.09	0.10	0.10	0.10

(a) All designs are for baseline parameters given in Table 3.4-I:

$$A = 6.5, R_T = 3.9 \text{ m}, r_p = 0.60 \text{ m}, V_p = 27.7 \text{ m}^3, r_w = 0.66 \text{ m}.$$

(b) $M_N = 1.36$, $\eta_{TH} = 0.35$, and water detritiation system cost $\simeq 5$ M\$.

(c) Gap between TF coil and OH coil, $G_{TF/OH} = 0.05$ m.

(d) Gap between TF coil and OH coil, $G_{TF/OH} = 0.31$ m.

(e) Asymmetric bipolar swing ($f_G \equiv I_{OH}^+/I_{OH}^- = 0.2$),

I_{OH}^+ subsequently decays to zero upon initiation of OFCD.

(f) Symmetric bipolar swing ($f_G \equiv I_{OH}^+/I_{OH}^- = 1$).

(g) Superconducting coils.

(h) Includes first wall, blanket, shield, and coils, but not FPC support structures.

(i) Costs reported in constant 1986-dollars, assuming 6 years construction time.

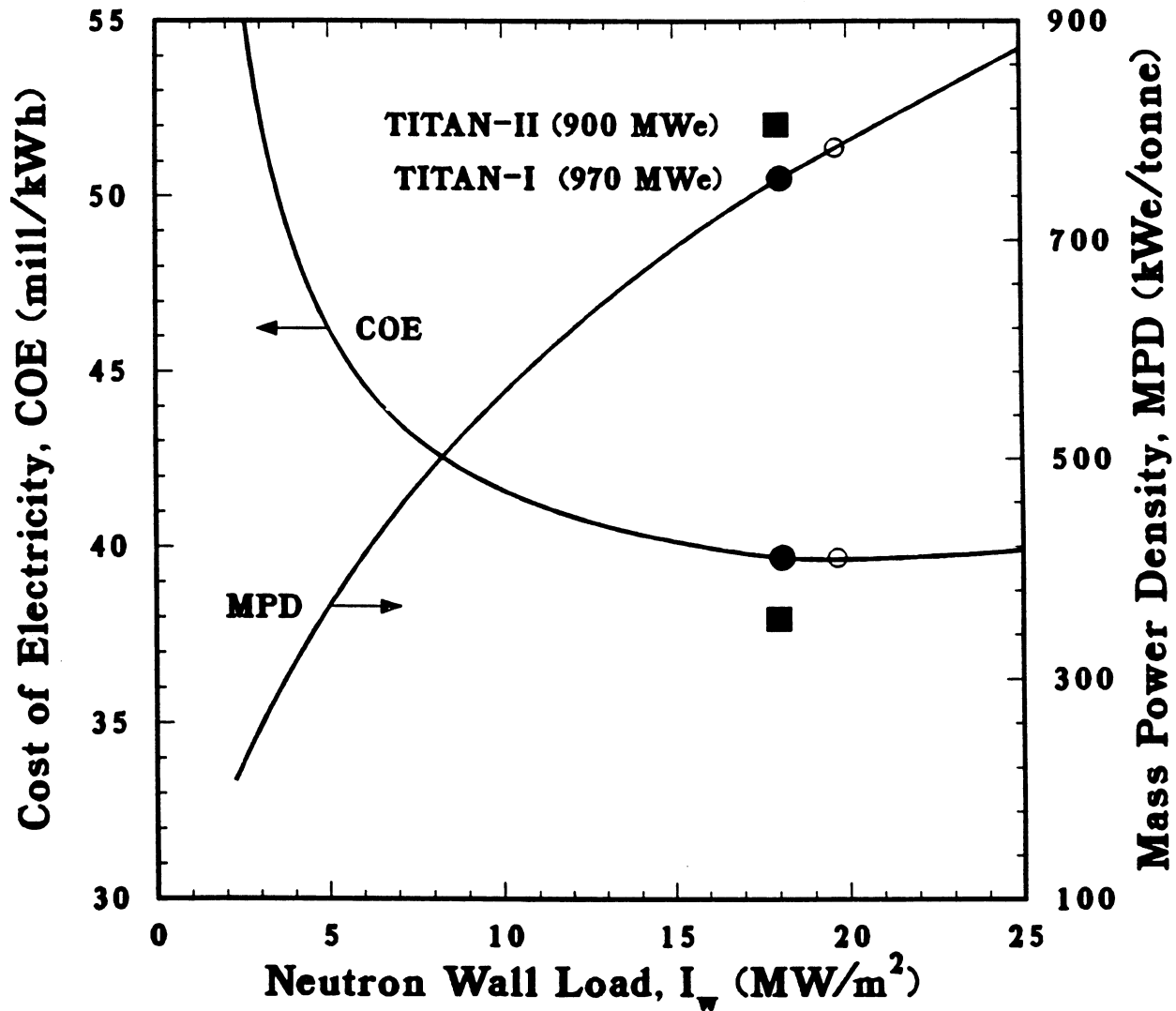


Figure 3.6-1. The COE and mass power density as functions of neutron wall load for the TITAN RFP reactor. Minimum-COE TITAN-I design point is indicated as an open circle. The near-minimum-COE reference design points for TITAN-I (filled circle) and TITAN-II (filled square) are also shown.

have a MPD in excess of 500 KWe/tonne, and a FPC engineering power density in the range 5 to 15 MWt/m³, representing improvements by factors of 10 to 30 compared with earlier fusion reactor designs. The FPC is a smaller portion of the total plant cost (typically about 12%) compared with 25% to 30% for earlier RFP designs [41,42]. Therefore, the unit direct cost, UDC (\$/kWe), is less sensitive to related physics and technology uncertainties.

The reference TITAN design points have been identified at a high neutron wall loading of $I_w \simeq 18 \text{ MW/m}^2$ with $A = 6.5$, $r_p = 0.60 \text{ m}$, and net power outputs of 970 MWe (TITAN-I) and 900 MWe (TITAN-II). The TITAN reference designs are summarized in Table 3.6-I. Previously reported TITAN-I results [43,44] are updated and superceded. Detailed subsystem design for TITAN-I and TITAN-II FPCs are reported throughout this report. The parameters of the TITAN-I and TITAN-II reference design points, based on detailed subsystem design, are included in Appendices A and B, respectively, following the DOE/OFE standard reporting format. The Appendices also include detailed cost tables and parametric systems code predictions of subsystem parameters for comparison with DOE/OFE tables.

Table 3.6-I.

SUMMARY OF REFERENCE DESIGNS OF TITAN REACTORS^(a)

Parameter	TITAN-I ^(b)	TITAN-II ^(c)
EF-coil option	SC ^(d)	SC ^(d)
DF-coil option	IBC ^(e)	Copper
TF-coil option	IBC ^(e)	Copper
Plasma Parameters		
Plasma current, I_ϕ (MA)	17.82	17.80
Plasma ion density, n_i (10^{20} m^{-3})	8.93	8.91
Plasma electron density, n_e (10^{20} m^{-3})	9.33	9.31
Poloidal field at plasma surface, $B_\theta(r_p)$ (T)	5.94	5.93
Thermal diffusivity, χ_E (m^2/s)	0.315	0.314
Fusion power density, P_F/V_p (MW/ m^3)	83.0	82.6
Plasma ohmic dissipation, P_{OHM} (MW)	28.5	28.5
Poloidal-Field Quantities		
OH-coil thickness, δ_{OH} (m)	0.27	0.37
Average minor radius of coil, r_{OH} (m)	1.56	1.37
OH-coil field, $B_{\theta c}$ (T)	2.28	2.61
OH-coil current density, j_{OH} (MA/ m^2) ^(f)	13.1	9.2
Mass of OH-coil set, M_{OH} (tonne)	343.	414.
EF-coil current density, j_{EF} (MA/ m^2)	19.2 ^(d)	20.6 ^(d)
Mass of EF-coil set, M_{EF} (tonne)	305.	247.
Poloidal-field stored energy, $W_{M\theta}$ (GJ)	5.2	4.1
OH-coil dissipation during back-bias (MW)	121.	107.
Toroidal-Field Quantities		
TF-coil thickness, δ_{TF} (m)	0.28 ^(e)	0.046
Average minor radius of coil, r_{TF} (m)	0.68	1.11
Mass of TF-coil set, M_{TF} (tonne)	41.	41.
Reversed-toroidal field, $-B_{\phi R}$ (T)	0.382	0.381
Toroidal-field stored energy, $W_{M\phi}$ (GJ)	0.16	0.43
TF-coil current density, j_{TF} (MA/ m^2)	1.64	9.2
Ohmic dissipation during burn, P_{TF}^Ω (MW)	27.6	13.6
Mass of DF-coil set, M_{DF} (tonne)	0.55	2.0
Ohmic dissipation in divertor, P_{DF}^Ω (MW)	142.	12.

Table 3.6-I (Cont'd)

Parameter	TITAN-I ^(b)	TITAN-II ^(c)
Engineering Summary		
Neutron first-wall loading, I_w (MW/m ²)	18.1	18.0
Engineering Q-value, $Q_E = 1/\epsilon$	4.02	7.20
Fusion power, P_F (MW)	2,301.	2,290.
Total thermal power, P_{TH} (MW)	2,935.	2,986.
Net electrical power output, P_E (MWe)	970.	900.
Fusion-power-core minor radius, r_s (m)	1.70	1.55
Masses (tonne)		
· First wall and blanket	41.	21.
· OH-coil "hot shield"	267.	106.
· EF-coil shield	325.	286.
· Total coil set	648.	704.
· Total fusion power core ^(g)	1,282.	1,117.
FPC power density, P_{TH}/V_{FPC} (MWt/m ³)	13.2	16.1
Mass power density, MPD (kWe/tonne) ^(g)	757.	806.
Cost Summary		
Cost of electricity, COE (mill/kWh) ^(h)	39.7	38.0
Unit direct cost, UDC (\$/kWe)	1,531.	1,543.
Total cost, TC (M\$)	2,396.	2,239.
FPC unit cost (\$/kg)	146.	119.
Fractions of total direct cost (TDC):		
· Reactor plant equipment, RPE/TDC	0.43	0.48
· Fusion-power-core cost, FPC/TDC ^(g)	0.13	0.10

(a) All designs are for baseline parameters given in Table 3.4-I:

$$A = 6.5, R_T = 3.9 \text{ m}, r_p = 0.60 \text{ m}, V_p = 27.7 \text{ m}^3, r_w = 0.66 \text{ m}.$$

(b) $M_N = 1.20$, $\eta_{TH} = 0.44$, and water detritiation system cost $\simeq 5$ M\$.

(c) $M_N = 1.36$, $\eta_{TH} = 0.35$, and water detritiation system cost $\simeq 140$ M\$.

(d) Superconducting coils.

(e) Integrated blanket coil (IBC).

(f) Symmetric bipolar swing ($f_G \equiv I_{OH}^+/I_{OH}^- = 1$),

I_{OH}^+ subsequently decays to zero upon initiation of OFCD.

(g) Includes first wall, blanket, shield, and coils, but not FPC support structures.

(h) Costs reported in constant 1986-dollars, assuming 6 years construction time.

REFERENCES

- [1] R. L. Hagenon and R. A. Krakowski, "Compact Reversed-Field Pinch Reactors (CRFPR): Sensitivity Study and Design-Point Determination," Los Alamos National Laboratory report LA-9389-MS (July 1982).
- [2] R. L. Hagenon, R. A. Krakowski, C. G. Bathke, R. L. Miller, M. J. Embrechts, *et al.*, "Compact Reversed-Field Pinch Reactors (CRFPR): Preliminary Engineering Considerations," Los Alamos National Laboratory report LA-10200-MS (August 1984).
- [3] C. Copenhaver, R. A. Krakowski, N. M. Schnurr, R. L. Miller, C. G. Bathke, R. L. Hagenon, *et al.*, "Compact Reversed-Field Pinch Reactors (CRFPR): Fusion-Power-Core Integration Study," Los Alamos National Laboratory report LA-10500-MS (August 1985).
- [4] R. L. Miller, C. G. Bathke, R. A. Krakowski, F. M. Heck, L. Green, J. S. Karbowski, *et al.*, "The Modular Stellarator Reactor: A Fusion Power Plant," Los Alamos National Laboratory report LA-9737-MS (July 1983).
- [5] R. L. Miller, R. A. Krakowski, C. G. Bathke, C. Copenhaver, N. M. Schnurr, A. G. Engelhardt, T. J. Seed, and R. M. Zubrin, "Advanced Tokamak Reactors Based on the Spherical Torus (ATR/ST)," Los Alamos National Laboratory report LA-10740-MS (June 1986).
- [6] J. D. Callen and R. A. Dory, "Magnetohydrodynamic Equilibria in Sharply Curved Axisymmetric Devices," *Phys. Fluids* 15 (1972) 1523.
- [7] D. J. Strickler, J. B. Miller, K. E. Rothe, and Y-K. M. Peng, "Equilibrium Modeling of the TFCX Poloidal Field Coil System," Oak Ridge National Laboratory report ORNL/FEDC-83/10 (April 1984).
- [8] H. M. Attaya and M. E. Sawan, "NEWLIT-A General Code for Neutron Wall Loading Distribution in Toroidal Reactors," *Fusion Technol.* 8 (1985) 609.
- [9] R. D. O'Dell, F. W. Brinkley, Jr., and D. R. Marr, "User's Manual for ONEDANT: A Code Package for One-Dimensional Diffusion-Accelerated Neutral-Particle Transport," Los Alamos National Laboratory report LA-9184-M (February 1982).
- [10] T. J. Seed, "TRIDENT-CTR User's Manual," Los Alamos Scientific Laboratory report LA-7835-M (May 1979).

- [11] J. F. Briesmeister, Ed., "MCNP- A General Monte Carlo Code for Neutron and Photon Transport, Version 3A," Los Alamos National Laboratory report LA-7396-M, Rev. 2 (September 1986).
- [12] A. K. Prinja and R. W. Conn, "An Axially Averaged Radial Transport Model of Tokamak Edge Plasma," *J. Nucl. Mater.* **128-129** (1984) 135.
- [13] D. Steiner, R. C. Block, and B. K. Malaviya, "The Integrated-Blanket-Coil Concept Applied to the Poloidal Field and Blanket Systems of a Tokamak Reactor," *Fusion Technol.* **7** (1985) 66.
- [14] N. Jarmie, R. E. Brown, and R. A. Hardenkopf, "Fusion-Energy Reaction $^2H(t, \alpha)n$ from $E_t = 12.5$ to 117 keV," *Phys. Rev. C* **29** (1984) 2031; also relevant Erratum in *Phys. Rev. C* **33** (1986) 385.
- [15] L. Woltjer, "A Theorem on Force-Free Magnetic Fields," *Proc. National Academy of Sciences* **44** (1958) 489.
- [16] J. B. Taylor, "Relaxation of Toroidal Plasma and Generation of Reversed Magnetic Field," *Phys. Rev. Lett.* **33** (1974) 1139.
- [17] V. S. Mukhovatov and V. D. Shafranov, "Plasma Equilibrium in a Tokamak," *Nucl. Fusion* **11** (1971) 605.
- [18] W. R. Smyth, *Static and Dynamic Electricity*, McGraw-Hill Book Company, NY (1939).
- [19] J. Kessner and R. W. Conn, "Space-Dependent Effects on the Lawson and Ignition Conditions and Thermal Equilibria in Tokamaks," *Nucl. Fusion* **16** (1976) 397.
- [20] J. Sheffield, R. A. Dory, S. M. Cohn, J. G. Delene, L. Parsly, D. E. T. F. Ashby, and W. T. Reiersen, "Cost Assessment of a Generic Magnetic Fusion Reactor," *Fusion Technol.* **9** (1986) 199.
- [21] S. Timoshenko and J. N. Goodier, *Theory of Elasticity*, 2nd edition, McGraw-Hill Book Company, Inc., New York (1951).
- [22] R. W. Conn (Chairman), "Panel X Report to the USDOE Magnetic Fusion Advisory Committee," University of California Los Angeles (May 8, 1985).
- [23] W. R. Hamilton, D. C. Keeton, and S. L. Thomson, "Cost Accounting System for Fusion Studies," Oak Ridge National Laboratory report ORNL/FEDC-85/7 (December 1985).

- [24] S. C. Schulte, T. L. Wilke, and J. R. Young, "Fusion Reactor Design Studies—Standard Accounts for Cost Estimates," Battelle Pacific Northwest Laboratory report PNL-2648 (May 1978).
- [25] S. C. Schulte, W. E. Bickford, C. E. Willingham, S. K. Ghose, and M. G. Walker, "Fusion Reactor Design Studies - Standard Unit Costs and Cost Scaling Rules," Pacific Northwest Laboratory report PNL-2987 (September 1979).
- [26] D. L. Phung, "A Method for Estimating Escalation and Interest During Construction (EDC and IDC)," in *Proc. 2nd Miami Conf. on Alternative Energy Sources*, Miami, FL (December 10-13, 1979).
- [27] S. L. Thomson, "Reference Cost Data for Fusion," Oak Ridge National Laboratory report ORNL/FEDC-86-8.
- [28] J. G. Delene, H. I. Bowers, and M. L. Meyers, "Nuclear Energy Cost Data Base," U. S. Department of Energy report DOE/NE-0041/3 (June 1985).
- [29] J. D. Lee (Ed.), "MINIMARS Conceptual Design: Final Report," Lawrence Livermore National Laboratory report UCID-20773 (September 1986).
- [30] I. Maya, K. R. Schultz, R. F. Bourque, E. T. Cheng, R. L. Creedon, J. H. Norman, *et al.*, "Inertial Confinement Fusion Reaction Chamber and Power Conversion System Study," GA Technologies report GA-A17842 (October 1985).
- [31] J. P. Holdren (Chairman), "Summary of the Report of the Senior Committee on Environment, Safety, and Economic Aspects of Magnetic Fusion Energy," Lawrence Livermore National Laboratory report UCRL-53766-Summary (September 1987).
- [32] C. C. Baker, M. A. Abdou, R. M. Arons, A. E. Bolon, C. D. Boley, J. N. Brooks, *et al.*, "STARFIRE – A Commercial Tokamak Fusion Power Plant Study," Argonne National Laboratory report ANL/FPP-80-1 (September 1980).
- [33] B. G. Logan, C. D. Henning, G. A. Carlson, R. W. Werner, D. E. Baldwin, W. L. Barr, *et al.*, "MARS Mirror Advanced Reactor Study Final Report," Lawrence Livermore National Laboratory report UCRL-53480 (July 1984).
- [34] B. Badger, I. N. Sviatoslavsky, S. W. Van Sciver, G. L. Kulcinski, G. A. Emmert, D. T. Anderson, *et al.*, "UWTOR-M: A Conceptual Modular Stellarator Power Reactor," University of Wisconsin report UWFD-550 (October 1982).

- [35] R. A. Krakowski, R. L. Hagenson, N. M. Schnurr, C. Copenhaver, C. G. Bathke, and R. L. Miller, "Fusion-Power-Core Integration Study for the Compact Reversed-Field Pinch Reactor (CRFPR): A Follow-On Study," *Nucl. Eng. and Design* **4** (1986) 75; also Los Alamos National Laboratory report LA-UR-85-3614.
- [36] R. A. Krakowski, R. L. Miller, C. G. Bathke, R. L. Hagenson, C. Copenhaver, and K. A. Werley, "Compact Reversed-Field Pinch Reactors (CRFPR)," *Proc. of IAEA Technical Committee Meeting and Workshop on Fusion Reactor Design and Technology*, Yalta, USSR (May 29 - June 6, 1986) **1** (1986) 331; also Los Alamos National Laboratory report LA-UR-86-1229.
- [37] M. K. Bevir and J. W. Gray, "Relaxation, Flux Consumption and Quasi Steady State Pinches," *Proc. RFP Theory Workshop*, Los Alamos National Laboratory April 28-May 2, 1980, Los Alamos National Laboratory report LA-8944-C (January 1982) 176.
- [38] K. F. Schoenberg, R. F. Gribble, and D. A. Baker, "Oscillating Field Current Drive for Reversed Field Pinch Discharges," *J. Appl. Phys.* **56** (1984) 2519.
- [39] D. S. Gelles, N. M. Ghoniem, and R. W. Powell, "Low Activation Ferritic Alloys Patent Description," University of California Los Angeles report UCLA/ENG-87-9 PPG-1049 (1987).
- [40] C. G. Bathke and R. A. Krakowski, "A Comparison Study of Toroidal-Field and Bundle Divertors for a Compact Reversed-Field Pinch Reactor," *Fusion Technol.* **8** (1985) 1616.
- [41] R. A. Krakowski, R. L. Miller, and J. G. Delene, "Directions for Improved Fusion Reactors," *Proc. IAEA Technical Committee and Workshop on Fusion Reactor Design and Technology*, Yalta, USSR (May 26-June 6, 1986) **1** (1986) 265; also Los Alamos National Laboratory report LA-UR-86-1386.
- [42] R. A. Krakowski, R. L. Miller, and R. L. Hagenson, "Prospects for Improved Fusion Reactors," in *Proc. 4th European Nuclear Conference (ENC-86)*, (June 1-6, 1986); also Los Alamos National Laboratory report LA-UR-86-641.
- [43] R. L. Miller, R. A. Krakowski, C. G. Bathke, K. A. Werley, and R. L. Hagenson, "Fusion Reactor Options and Alternatives for the RFP," *Fusion Technol.* **10** (1986) 1159.

- [44] R. L. Miller, "The TITAN Reversed-Field Pinch Reactor: Design-Point Determination and Parametric Studies," in *Proc. 12th IEEE Symp. Fusion Engineering*, Monterey, CA (October 12-16, 1987).